PHYSICAL REVIEW B

CONDENSED MATTER

THIRD SERIES, VOLUME 46, NUMBER 17 1 NOVEMBER 1992-I

Charge oscillations and structure for alkali-metal-doped polyacetylene

R. H. Baughman, N. S. Murthy, and H. Eckhardt
Allied-Signal Inc., Research and Technology, Morristown, New Jersey 07962

M. Kertesz
Department of Chemistry, Georgetown University, Washington, D.C. 20057

(Received 2 January 1992)

Symmetry-breaking structural and charge oscillations are calculated for $(C_pH_p)^-$ lattices ($p=5$ to 9) and used to predict Coulombic expansion coefficients, x-ray photoelectron spectra, and crystallographic features that can be compared with experimental results. Extension of these predictions to other dopant concentrations is provided by derived analytical expressions. The parameters for the infinite lattices are derived from oligomer-ion results obtained from modified neglect of differential overlap calculations. Such calculations on oligomer ions with different parametrizations provide essentially identical changes in charge and structural parameters upon doping and these changes are in excellent agreement with the results of infinite-chain calculations. The degree to which oligomer-ion segments retain the structural parameters of charged arrays for the infinite lattice is remarkable. Derived geometries and charge distributions indicate two different types of charged defects, solitons (or antisolitons) and split solitons (or split antisolitons), and the geometry and charge distribution of the latter defects is shown to correspond to the average of those for two soliton lattices that have a relative shift of two CH units. At least in the absence of an external Coulomb field, soliton and split-soliton lattices for p odd are quasidegenerate, and the lattices for p even consist of alternating sequences of solitons and split antisolitons. Large oscillations in local chain-axis direction are predicted, which is a consequence of both oscillations in bond angles and the nonequivalence of even (and odd) bond lengths. Including these effects provides predicted Coulombic expansion coefficients that are in good agreement with observations for Na-doped polyacetylene. Much smaller bond-angle oscillations are predicted for anion lattices than for cation lattices, which can be at least partially explained by Coulomb effects. Observed ^{13}C NMR chemical shifts are consistent with predictions for oligomers, and good agreement is obtained between calculated and observed x-ray photoelectron spectra for sodium-doped polyacetylene. Emphasis is placed on the results of crystallographic studies of alkali-metal-doped polyacetylene and on the relationship between the experimentally derived symmetry breaking in interchain packing and the molecular symmetry breaking predicted by theory. Since presently available experimental data are insufficient for complete determination of structure, the present theoretical results can be useful for refinements in the interpretation of these data, as well as for refined crystal-packing calculations.

I. INTRODUCTION

Early work indicated that polyacetylene doped with heavy alkali metals has a channel structure in which there are two polyacetylene chains per alkali-metal ion column.[1] The proposed crystal packing is tetragonal or pseudotetragonal with each alkali-metal ion column coordinated with four polyacetylene chains. Various investigations have supported these basic features,[2-15] but various structural distortions have been recently reported[8-13] that result in a decreased structural symmetry. Also, hexagonal or pseudohexagonal structures have been reported for Li-doped[16] and for Na-doped[17,18] polyacetylene. Evaluation of the interactions that provide symmetry-breaking distortions for these structures is important for understanding charge transport, band structure, and the nature of charge lattices in doped polyacetylene.

This work examines the nature and origin of symmetry breaking in polyacetylene heavily doped with alkali metals. One hypothesis is that symmetry breaking results from oscillations in the charge and geometry associated with backbone carbons due to formation of a soliton lattice. In order to evaluate this hypothesis, the magnitude

and symmetries of backbone charge oscillations are calculated and compared with experimental results. Section II discusses the experimentally derived crystal structures for polyacetylene heavily doped with alkali metals. Section III presents calculated results on backbone charge oscillations and dimensional changes that provide symmetry breaking, Sec. IV compares properties predicted using these parameters with experimental results, and Sec. V presents conclusions regarding the nature and origin of symmetry breaking in polyacetylene.

Calculation of charge distribution and geometry for the polyacetylene chain as a function of dopant level is an important part of this work. It is believed that these calculated results will be useful for future investigations of structure-property relationships in doped polyacetylene. For this reason, considerable effort is devoted to deriving the most reliable set of parameters obtainable by the present semiempirical theoretical methods and to establishing relationships between these parameters. To the extent possible, the predictions of the theoretical calculations are compared with experimental results in order to assess reliability.

II. PROPOSED STRUCTURES FOR POLYACETYLENE DOPED WITH ALKALI METALS

The structures for alkali-metal-doped polyacetylene are complicated because of variations in the concentration of alkali-metal ions in the ion columns, as well as the number of polymer chains per alkali-metal ion column. The ion-column filling factor is denoted by the index n (corresponding to the number of chain carbons in a chain length equal to the average intracolumn ion-ion separation) and the number of polymer chains per alkali-metal ion column is denoted by the index m. Hence, these structures are designated for alkali metal M by $(C_nH_n)_mM$, where $m=2$ for the tetragonal or pseudotetragonal phase at the highest dopant concentrations, $m=4$ for the phase that results from dedoping, and $m=3$ for the hexagonal or pseudohexagonal phase.[2,3,15]

Model A in Fig. 1 shows the tetragonal or pseudotetragonal packing mode proposed by Baughman, Murthy, and Miller[1] for polyacetylene heavily doped with sodium, potassium, rubidium, or cesium. Depending upon the size of the alkali-metal ion, variations on this basic packing mode are expected. However, independent of the size of the alkali-metal ion in this series, common structural features are observed. The alkali-metal ions form columns, each of which are surrounded by four polymer chains. In turn, each polymer chain coordinates two alkali-metal ion columns, so these structures contain two polymer chains per alkali-metal ion column. The basal-plane dimension of the tetragonal or pseudotetragonal cell increases with increasing van der Waals diameter ions above potassium, producing unit-cell parameters in chain-axis projection (a') of 6.0±0.1 Å for sodium, 5.98±0.05 Å for potassium, 6.19±0.07 Å for rubidium, and 6.43±0.07 Å for cesium.[1] Assuming that the nearest-neighbor alkali-metal columns are shifted in the chain-axis direction so as to minimize electrostatic repulsions, the corresponding basal-plane unit-cell parameter

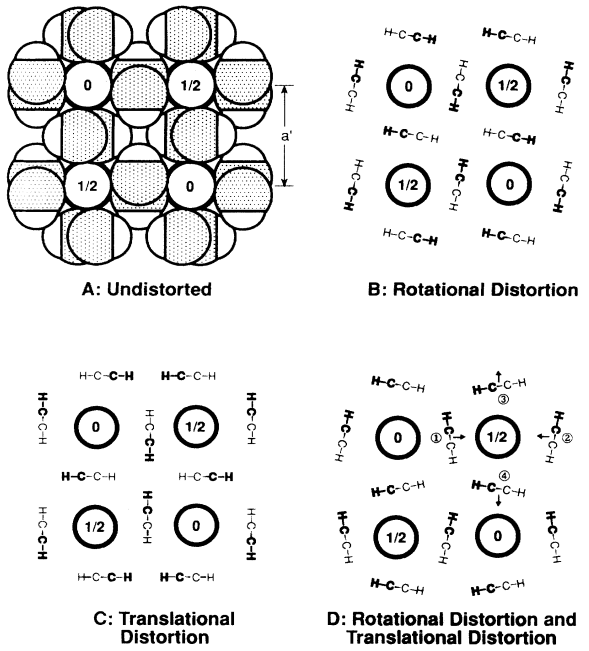

FIG. 1. Chain-axis projections for various structural models for the tetragonal or pseudotetragonal $(C_nH_n)_4K$ phases. In the representation used for model A, which shows van der Waals dimensions for all atoms, the carbons correspond to the dot-highlighted circles and the small intersecting circles correspond to the attached hydrogens. The columns of potassium ions are shown in all models as the circles having the van der Waals radius of K^+ and a number to indicate the relative chain-axis heights of neighboring ion columns for a body centering of columns.

is $a=\sqrt{2}a'$ for the smallest possible tetragonal unit cell.

The above mentioned early work on alkali-metal-doped polyacetylene assumed bond-centered coordination of potassium, rubidium, and cesium ions. More recent work[8-13] suggests the presence of structural distortions that eliminate this bond centering. Although the quality of obtainable x-ray-diffraction data has increased because of materials improvements, the quality of this data is still not sufficient to provide full structural details. Nevertheless, there is evidence that deviations from bond-centered coordination occur.

Chen *et al.*,[13] Saldi, Lelaurian, and Billaud,[12] and Aime *et al.*[8] have all proposed structural models for heavily potassium-doped polyacetylene which, although differing, provide a common feature—nonequivalent distances in projection between alkali-metal columns and polyacetylene chain carbons on opposite sides of the polymer backbone. Model C in Fig. 1 shows the structural distortion reported by Chen *et al.*[13] for potassium-doped polyacetylene. This distortion corresponds to a major shift of chain position by 0.36±0.08 Å along a', which is about one-half of the separation of neighboring chain carbons in chain-axis projection. Chen *et al.*[13] have reported the same type of distortion for heavily rubidium-doped polyacetylene, corresponding to a chain position shift of 0.31±0.05 Å. Since in the absence of such a distortion

the alkali-metal ion column would be at a midpoint position with respect to the polymer chain, the consequence of these shifts is a decrease of the average carbon–column separation for carbons on one side of the chain at the expense of carbon atoms on the other side of the chain. Model D in Fig. 1 shows the structural distortion proposed by Saldi, Lelaurain, and Billaud[12] for polyacetylene doped with potassium, rubidium or cesium. The polyacetylene chains rotate by a small angle ϕ and chains 1 and 2 are brought slightly closer to the center of the cell, while chains 3 and 4 are slightly shifted away from the center of this cell. As related to the separations of alkali-metal columns and the carbon atoms on opposite sides of the chain backbone (measured in chain-axis projection), the consequence of this symmetry breaking is similar to that for the Chen *et al.*[13] model: The distance between alkali-metal column and carbon atoms is increased on average for carbon atoms on one side of the chain and decreased on average for carbon atoms on the opposite side of the chain. Aime *et al.*[8] were the first to propose structural distortions for K-doped polyacetylene. Based on their neutron-diffraction data, Aime *et al.*[8] claimed that the "tetragonal" phase is really monoclinic, with axial lengths and interaxial angle very close to those for the tetragonal cell (5.98 Å, 5.96 Å, and $\beta=91.7°$ before thermal annealing and 5.94 Å, 5.93 Å, and $\beta=90.8°$ after thermal annealing). The packing mode is very similar to that proposed by Baughman, Murthy, and Miller,[1] except for these very small deviations in unit-cell parameters and a 10–20° rotation of the polymer chains. Later work has not supported the above mentioned changes in unit cell reported by Aime *et al.*,[8] but the chain rotations proposed by these authors (illustrated by model B in Fig. 1) are also a component of the somewhat-different model (model D of Fig. 1) proposed by Saldi, Lelaurain, and Billaud.[12] The rotation angle needed to bring the alkali-metal ion column on top of one side of a straight, planar transpolyacetylene chain (7°) is reasonably close to the range of rotation angles (10–20°) that provided the best fit to the data of Aime *et al.*[8] However, we will later show that doped polyacetylene chains can significantly deviate from the conventional view of a straight chain. Also, the most recent work of Saldi, Lelavrain, and Billaud[12] provides support for the Chen *et al.*[13] model of a translational distortion (model C in Fig. 1).

Upon decreasing the dopant concentration, the two chain per column tetragonal-like structure for potassium-doped polyacetylene transforms to a structure in which each alkali-metal column is again coordinated with four surrounding chains. However, each polymer chain is coordinated with only one alkali-metal column in the lower dopant concentration phase, so there are now four polymer chains per alkali-metal ion column.[6,11,12] Heiney *et al.*[11] have concluded from x-ray diffraction data that symmetry breaking occurs for this $(C_nH_n)_4K$ phase and that this symmetry breaking is directly analogous to that reported by Chen *et al.*[13] for the $(C_nH_n)_2K$ phase. Despite the coordination of each chain with only one alkali-metal column in the former structure, the arrangement of four polymer chains about each alkali-metal ion column is reported to be essentially the same as for the latter structure.

When the size of the alkali-metal ion is small compared with the van der Waals width of the polymer chain, the structure stable at high dopant concentrations is hexagonal or pseudohexagonal rather than tetragonal or pseudotetragonal. Similar hexagonal structures have been reported for both Li-doped polyacetylene[16] and Na-doped polyacetylene,[17,18] Na-doped poly(*p*-phenylene),[19] and both Na-doped and K-doped poly(*p*-phenylene vinylene).[20,21] As illustrated by the structure proposed for Li-doped polyacetylene (Fig. 2), these structures contain an alkali-metal column surrounded by three polymer chains as the structural motif. In contrast with the case for the two chain per column tetragonal or pseudotetragonal phases, each polymer chain is coordinated with only one alkali-metal ion column. Despite this difference, which has major consequences for symmetry arguments, the same fundamental question arises as for the tetragonal or pseudotetragonal phases: Do symmetry-breaking deviations from idealized structures occur that minimize carbon-ion separations for carbons on one side of a chain at the expense of carbon-ion separations for carbons on the opposite side of the chain? Heiney *et al.*[11] have already reported for $(C_nH_n)_3Li$ that symmetry-breaking chain offset occurs, which is analogous to that for the $(C_nH_n)_2K$ and $(C_nH_n)_4K$ phases.

The following picture of structural evolution during potassium doping is suggested by diffraction,[1–16] electrochemical potential,[2,3,22–27] Raman,[28–31] and electron-spin resonance[23–25] measurements. The potassium doping of polyacetylene initially proceeds as a two-phase process between a dopant concentration y of zero and about 6% to convert essentially undoped polyacetylene into the four chain per column phase, $(C_4H_4)_4K$. Increasing dopant concentration results in channel filling until a composition of approximately $(C_3H_3)_4K$ is reached. This phase with such high column filling appears to be unsta-

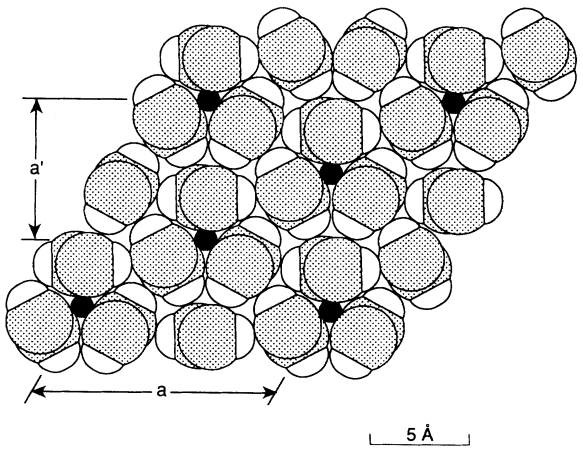

FIG. 2. Chain-axis projection for the structural model proposed by Murthy, Shacklette, and Baughman (Ref. 14) for Li-doped polyacetylene. The structure is hexagonal or pseudohexagonal. The indicated a' is a unit-cell parameter that provides the periodicity in chain-axis projection and the larger unit-cell parameter a corresponds to the basal-plane unit-cell parameter for the three-dimensional structure.

ble with respect to formation of the tetragonal or pseudotetragonal phase $(C_4H_4)_2K$. Increasing dopant concentration results in filling of the columns in the latter phase until a final composition of approximately $(C_3H_3)_2K$ is obtained. According to electrochemical results,[22] dedoping proceeds similarly, except the $(C_nH_n)_2K$ phase is metastably retained until n is approximately 5 and this phase directly transforms on decreasing dopant level to the stable $(C_4H_4)_4K$ phase. As will be discussed later, we are unaware of diffraction evidence for commensurate phases other than for $n=4$, so the above use of phrases denoting approximately $n=3$ and approximately $n=5$ should be noted.

The intracolumn and intercolumn separations between alkali-metal ions, as well as the relationship between alkali-metal ion and polymer-chain coordinates, are expected to be dominated by electrostatic interactions. The simplest approximations are that all carbons (and all CH units) have the same charge and that all even-carbon atoms (and all odd-carbon atoms) coincide in a projection down the chain-axis direction. Even though the breakdown of these approximations provides an emphasis of this paper, it is useful to consider those structures that might result if this approximation were valid. If all carbon atoms had the same negative charge, electrostatic energy could be minimized by achieving maximum nearest-neighbor coordination of the negatively charged carbons and the positively charged alkali-metal ions. This would result for the $(C_4H_4)_2M$ structure if each alkali-metal ion were coordinated at the midpoint of carbon-carbon bonds in each of four neighboring chains, as illustrated in Fig. 3 and in Model A of Fig. 1. In such a case, where all polymer chains have a carbon at the same chain-axis coordinate, each alkali metal is nearest neighbor to eight carbon atoms. Also, intercolumn inter-ion separation is maximized, since ions in neighboring columns are shifted with respect to one another in the chain-axis direction by one-half of the alkali-metal–alkali-metal intracolumn separation. Such array of alkali-metal ions is referred to as a body-centered array. Note that the $(C_4H_4)_2M$ structure with body centering and with bond-centered alkali-metal coordination is the only structure in which there is any possibility for the equivalence of all CH units.[2] Also, the $(C_4H_4)_2M$ structure with body centering and with alkali-metal ions equivalently placed with respect to two C-C bonds in the chain provides the only case where all C-C bonds in the chain have the possibility to be equivalent. We will see that such equivalence of carbon atoms or C-C bonds is excluded because of fundamental structural features of charged polyacetylene chains. Analogous structures containing body-centered ion arrays could generally be described for $(C_nH_n)_2M$ where n is even, but $n=2$ and $n=6$ provide, respectively, too high and too low a column filling factor to result in stable structures.

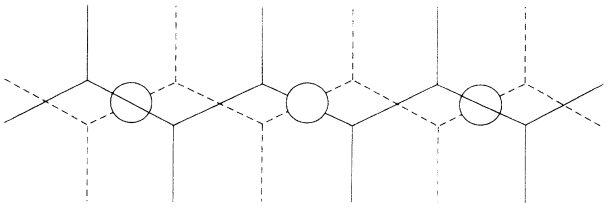

FIG. 3. Polyacetylene chains on top (solid lines) and underneath (dashed lines) a column of alkali-metal ions (end circles). The central circle represents an alkali-metal ion which is in a column of alkali-metal ions that is located on top of the former chain. Bond-centered coordination of alkali-metal ions is pictured in this model for $(C_4H_4)_mM$, which provides commensurate polymer-chain and alkali-metal ion periodicities.

Experimental data indicate that channel filling corresponding to $n=4$ can be preferred for $(C_nH_n)_mM$ phases, which suggests a lock in of chain-channel commensurability. Murthy, Shacklette, and Baughman[32] observed an intense meridional reflection at 2.50 Å for the two-chain per column, tetragonal-like phase at a dopant concentration y of about 0.12, but not at substantially higher doping levels. This spacing equals the chain length per C_2H_2 unit (L), after correction for the expansion caused by doping. The diffraction contribution from successive CH units are nearly 180° out of phase for this diffraction line. Consequently, the observed high diffraction intensity must be largely due to columns of potassium that have an intracolumn spacing of four CH units and a body-centered shift between neighboring ion columns. This means that $(C_4H_4)_2K$ exists as a special stoichiometric phase and that alkali-metal ion columns undergo a body-centered shift in this phase so as to minimize electrostatic energy. Such body centering provides the intense observed diffraction spacing at L, but results in out-of-phase scattering at $2L$. Relevant to the stability of structures having $n=4$, it is important to note that Mathis *et al.*[7] observed a meridional x-ray-diffraction streak at $2L$ for an overall dopant level of $y=0.01$ to 0.10, which corresponds to the independent scattering of alkali-metal ion columns with $n=4$. The stability of such a structure down to near zero doping levels speaks of the importance of chain-column commensurability for $n=4$.

The special importance of $n=4$ column filling has also been demonstrated for other alkali-metal ions, including sodium, rubidium, and cesium. Saldi, Lelaurain, and Billaud[12] have provided diffraction evidence that the polymer chains and alkali-metal columns are commensurate and the column filling factor corresponds to $n=4$ for sodium-, potassium-, rubidium-, and cesium-doped polyacetylene at $y \leq 0.125$. These results are consistent with the conclusions of various other researchers[7,15,32] and suggest stoichiometric compositions arising from chain-column commensurability for $(C_4H_4)_4M$, $(C_4H_4)_3M$, and $(C_4H_4)_2M$ phases. At the highest dopant level obtained for the $(C_nH_n)_2M$ structure, Saldi, Lelaurain, and Billaud[12] reported diffraction data which are consistent with body centering of the alkali-metal ion columns. However, the intracolumn, interion spacing at the highest doping level for potassium-, rubidium-, and cesium-doped polyacetylene (3.98 Å, 4.02 Å, and 4.07 Å, respectively) are longer than the 3.75 Å spacing expected for the commensurate phase $(C_3H_3)_2M$. Mathis *et al.*,[7] Ma *et al.*,[4] and Leitner *et al.*[14] have also reported incommensurability between chain-axis and ion-column periodicities at the highest doping level for K-doped and Cs-doped polyacetylene. The reported ion-ion separations agree with the above mentioned results of Saldi,

Lelaurain, and Billaud.[12] Also, Ma *et al.*[4] and Chen *et al.*[13] concluded that heavily cesium-doped polyacetylene and heavily rubidium-doped polyacetylene have body-centered alkali-metal ion columns and that the polymer chains and alkali metal columns form two interpenetrating three-dimensional lattices that are incommensurate only in the chain-axis direction.

The summary of the x-ray-diffraction results is that $(C_4H_4)_mM$ structures with commensurate column and chain-axis periodicities occur for the $m=2$, 3, and 4 phases. For the $m=3$ and $m=4$ phases, the degree of intercolumn correlation in ion chain-direction coordinates is low or negligible. However, for the $n=2$ tetragonal or pseudotetragonal phase, strong intercolumn correlation occurs, which provides body-centered shifts between neighboring ion columns. Such correlated shifts for the tetragonal or pseudotetragonal $m=2$ phase appear to occur independent of the column filling factor. The only presently observed cases in which chain-axis and ion-column periodicities are commensurate are provided when $n=4$. An additional complication is provided by the report of Winokur *et al.*,[17] which claims that continuous evolution in the chain-to-column number ratio occurs in sodium-doped polyacetylene.

We herein assume that the alkali metals in polyacetylene are completely ionized. Experimental support for this assumption is provided by the nuclear-magnetic resonance (NMR) measurements of Bernier *et al.*[33] on lithium-doped and on sodium-doped polyacetylene. The NMR resonances due to lithium and sodium are unshifted with respect to standard ionic reference compounds, indicating that the dopants are in a purely ionic state. The situation is more complicated for cesium-doped polyacetylene, since two NMR lines are observed, both of which are shifted with respect to the NMR line of the ionic reference compound.

III. CHARGE AND STRUCTURAL OSCILLATIONS IN POLYACETYLENE CHAINS

A. Theoretical methods and comparison of results with experiments on monoanions

Semiempirical quantum-chemical methods will be used to calculate atomic charges and molecular geometries for polyenes having the form $H(CH)_uH$. Since we are interested in predictions for a soliton lattice, the number of charges placed on the molecule is odd when u is odd and even when u is even. The methods used are modified neglect of differential overlap[34] (MNDO) and the same type of calculation with Austin model 1 (AM1) parametrization,[35] which are known to provide electrostatic potentials that are in good agreement with *ab initio* Slater-type orbital, three-Gaussian expansion (STO-3G) basis-set calculations.[36] A similar approach was used by Boudreaux *et al.*[37] and Chance *et al.*[38] in their important early evaluation of charge distribution and geometry for isolated solitons, polarons, and bipolarons in polyacetylene. Although atomic charges designed to reproduce quantum chemically derived electrostatic potentials are more reliable for electrostatic energy calculations than the Mulliken charges calculated in the present work,[36,39] we will see that these calculated Mulliken charges are consistent with observed NMR chemical-shift data on diphenylpolyene anions. It is important to realize that atomic charge is not a uniquely defined quantity and that the most appropriate definition for comparison with experimentally derived charges can depend upon the experimental method. Atomic charges are herein expressed in units so that -1 corresponds to the charge of an electron.

Tolbert and Ogle[40–42] concluded that AM1 calculations provide qualitatively correct carbon-to-carbon charge variations for polyene anions, but overestimate the magnitude of charge on carbon by a factor of about two. We herein show that both the MNDO and AM1 calculated carbon charges are quantitatively consistent with the observed shifts for these anions and that any differences between calculated charges and those derived from chemical shifts are obscured by uncertainties in the relationship used to derive experimental charges from observed chemical shifts. Specifically, Tolbert and Ogle used the approximation that

$$\delta_c=\alpha q+\delta_0 , \tag{1}$$

where α and δ_0 are constants, q is the charge on a carbon, and δ_c is the corresponding chemical shift. The derivation of the constants α and δ_0 is controversial. The above authors calculated carbon charges from the observed chemical shifts using $\alpha=187.3$ and $\delta_0=132.7$, which they obtained from the observed linear correlation between average chemical shift for diphenylpolyene anions of differing length and the average charge per carbon. Such analysis effectively assumes that the sum of all charges on carbon atoms equals -1, which neglects charge contributions from the hydrogen atoms, which are generally believed to be appreciable. Also, Tolbert and Ogle note that they would have obtained a much lower value of $\alpha=124.5$ if they had corrected for local anisotropy effects using chemical-shift data on neutral polyenes. Additionally, these authors point out that there is a strong correlation between their experimentally derived charge densities for the diphenylpolyene anions and those that they calculate using AM1. We find that the chemical shifts observed by Tolbert and Ogle for the longest diphenylpolyene anion investigated are linearly correlated with those derived from either MNDO or AM1 calculations for this anion. The correlation coefficient r is slightly better for the AM1 results ($r=0.993$) than for the MNDO results ($r=0.972$), suggesting that the AM1 results might be more reliable. The derived coefficients are $\alpha=80.22$ and $\delta_0=136.6$ from the AM1 calculation and $\alpha=74.66$ and $\delta_0=130.89$ from the MNDO calculation. Note that these coefficients for α are slightly closer to the anisotropy-corrected slope ($\alpha=124.5$) than to the value used by Tolbert and Ogle (187.2). Table I provides a comparison of the charges on the carbons calculated by AM1 and the charges obtained from the experimental chemical shifts assuming the above α and δ_0 obtained from the correlation between AM1 calculated charges and the observed chemical shifts. While the total charges on CH units obtained by AM1 and MNDO calculation methods are in good agreement, the AM1 method places

TABLE I. Comparison of AM1-calculated carbon charges, q(AM1), and those derived from observed ^{13}C chemical shifts, q(NMR), for the -1 anion of the diphenylpolyene $H_4C_6(CH)_{13}C_6H_4$. Carbon atoms are numbered starting from the carbon in the center of the polyene sequence (C1s) and proceeding through six carbons in the polyene backbone (C2 to C7) to the aromatic ring (C8, C9, C10, and C11 for the ipso, ortho, meta, and para carbons, respectively).

	C1	C2	C3	C4	C5	C6	C7	C8	C9	C10	C11
q(AM1)	−0.364	0.030	−0.350	0.013	−0.313	−0.016	−0.257	0.025	−0.153	−0.126	−0.169
q(NMR)	−0.363	0.030	−0.349	0.025	−0.300	−0.054	−0.270	0.046	−0.164	−0.103	−0.176

more positive charge on the hydrogen atoms. This provides the differences in derived values of α and δ_0 for these calculation methods. We will later demonstrate that the AM1 and MNDO evaluations for various anion polyacetylene lattices provide the same changes in carbon charges with respect to the carbon charge calculated for the neutral polymer. Since the above described linear correlation exists between AM1 charge and observed chemical shifts, the availability of reliable, independently derived values of α and δ_0 would permit correction of AM1-calculated carbon charge if such correction should be required. For example, if we assume that the local-anisotropy-corrected α discussed by Tolbert and Ogle[38] is valid, then the differences in charge between different carbons that we calculate by AM1 and MNDO are factors of 1.55 (AM1) and 1.66 (MNDO) too large (corresponding to the ratio of our α values to the local-anisotropy-corrected value[42] of 124.5).

B. General features of the lattice calculations

Charge distribution and geometry was derived for a soliton lattice in polyacetylene at dopant concentration y, $[(CH)_{1/y}]^-$, from AM1 and MNDO calculations on $[H(CH)_uH]^{x-}$ anions, where $u=23$, 25, 33, 35, 37, 39, or 41 and $x=3$, 5, or 7 for u odd and $u=16$ or 32 and $x=4$ or 6 for u even. Confirmation that the derived charges and geometry are not dominated by chain-end effects was obtained for various combinations of u and x by comparison of soliton parameters derived from calculations on different-length anions. Except for requiring the backbone to be planar and all trans, no constraints were placed on backbone geometry during geometry optimization. Relaxing this planarity constraint provided no significant change in calculated charge distribution or geometry for the anions. For example, the maximum deviation from dihedral angles of 180° was 0.09° for AM1 calculations of $[H(CH)_{33}H]^{5-}$. Additional checks on the validity of polymer parameters derived from oligomer calculations were provided by (1) the symmetry or near symmetry of charge distribution and backbone geometry with respect to soliton and antisoliton centers, (2) the near-unity value of total charge on the integer number of CH units that can be associated with a charged soliton, and (3) the agreement between the charge distribution and geometry derived from the oligomer results and corresponding infinite-chain calculations for selected soliton lattices. The observation of Tolbert and Ogle[42] that the NMR chemical shifts are independent of the size and nature of the counter cation for the oligomers suggests that the present isolated-chain calculations should provide the basic structural features appropriate for the polymer chain in a three-dimensional array with other chains and counterions.

The simplest type of soliton lattice is obtained when the number of CH units per unit charge ($p=y^{-1}$) is an odd integer. In such case, the soliton lattice can be described by charged solitons (S_1) and charge antisolitons (S_{1a}), which alternate every p carbon atoms. Charged solitons and charged antisolitons denote charged π-phase shift kinks which provide a maximum-magnitude excess charge at a central carbon atom and carbon-carbon bonds on both sides of this central carbon which are longer than bonds that are next nearest neighbor to this carbon. A second type of charged soliton and charged antisoliton is also provided by the present calculations. This type of soliton has previously been described by Takahashi and Fukutome[43] and is reported by these authors to have nearly the same energy as a conventional soliton. Also, Strafstrom has derived the same type of defect from calculations using a Su-Schrieffer-Heeger Hamiltonian including terms for π-electron hopping and σ-bond repulsion.[44] Such charged solitons (or antisolitons) differ from conventional charged solitons in that (1) the maximum magnitude excess charge is on the carbon atoms on either side of a weakly charged carbon atom that is at the defect center and (2) carbon-carbon bonds to this central carbon are shorter than bonds that are next nearest neighbor to this carbon. We designate this second type of soliton (or antisoliton) as a split soliton (or split antisoliton), since such a defect might be viewed as a resonance average of structures in which a conventional soliton is on either the next carbon to the left or the next carbon to the right of the central carbon of the split soliton. The split soliton and the split antisoliton are designated S_2 and S_{2a}, respectively. This second type of soliton results from the displacement of a conventional soliton by one CH unit in the chain-axis direction.

C. Odd-carbon soliton lattices

Initial calculations were performed using both AM1 and MNDO methods in order to derive charge distribution and geometry for the soliton lattices $(C_9H_9)^-$ and $(C_9H_9)^+$ from calculations on $[H(CH)_{23}H]^{3-}$ and $[H(CH)_{23}H]^{3+}$, respectively. As shown in Tables II–IV, these calculations indicate the consistency between results obtained by AM1 and MNDO methods when a suitable basis for comparison is made. Also, these calculations indicate both areas in which there is correspon-

TABLE II. Comparison of CH charges calculated by AM1 and MNDO for the soliton lattice of $(C_9H_9)^-$ and $(C_9H_9)^+$ using the charge distributions for $[H(CH)_{23}H]^{3-}$ and $[H(CH)_{23}H]^{3+}$. The labeling of atoms is indicated in Fig. 4 for Tables II–VIII.

	$(C_9H_9)^-$		$(C_9H_9)^+$	
	AM1	MNDO	AM1	MNDO
$q(C_1H_1)$	−0.327	−0.352	0.308	0.338
$q(C_2H_2)$	0.078	0.095	−0.062	−0.086
$q(C_3H_3)$	−0.271	−0.288	0.256	0.278
$q(C_4H_4)$	0.009	0.020	−0.002	−0.019
$q(C_5H_5)$	−0.142	−0.143	0.138	0.143
$q(H)$[a]	0.084(11)	0.012(13)	0.163(9)	0.085(10)
$\Delta q(H)$[b]	−0.041	−0.038	0.038	0.035

[a] $q(H)$ is average charge on hydrogens. Estimated standard deviations in the least significant digit are shown in parentheses.
[b] $\Delta q(H)$ is the deviation of $q(H)$ for the soliton lattice from $q(H)$ for neutral polyacetylene. $q(H)$ is 0.125 for AM1 and 0.050 for MNDO, using calculated values near the center of $H(CH)_{32}H$.

dence and areas in which there are major differences in calculated parameters for negative and positive soliton lattices. For parameters that lie in the former area, we will use this correspondence for comparison of presently calculated parameters for anion lattices of polyacetylene with those previously calculated using different quantum-chemical methods for cation lattices of this polymer.

AM1 and MNDO calculations on $[H(CH)_{23}H]^{3-}$ and $[H(CH)_{23}H]^{3+}$ indicate symmetries and quasisymmetries that are consistent with those indicated in Fig. 4 for the $(C_9H_9)^-$ lattice. Specifically, the central carbon atom and the ninth carbon atoms on either side of this center have maximum charge and the calculated geometry and charge distribution provides nearly a mirror plane symmetry about this central carbon and nearly a center of symmetry at the midpoints between the central carbon and the ninth carbon on either side. Furthermore, the amount of charge on CH units between these quasi

TABLE III. Comparison of calculated deviations $\Delta(C_iC_j)$ of bond lengths C_i-C_j for the soliton lattice from the average value for the neutral chain (1.3954 Å by AM1 and 1.4099 Å by MNDO from the average of single and double bond lengths near the center of $H(CH)_{32}H$). Bond lengths for the soliton lattice of $(C_9H_9)^-$ and $(C_9H_9)^+$ are calculated using the AM1 and MNDO calculated bond lengths for $[H(CH)_{23}H]^{3-}$ and $[H(CH)_{23}H]^{3+}$, respectively.

	$(C_9H_9)^-$		$(C_9H_9)^+$	
	AM1	MNDO	AM1	MNDO
$\Delta(C_1C_2)$	0.003 Å	0.004 Å	0.010 Å	0.011 Å
$\Delta(C_2C_3)$	−0.023	−0.026	−0.020	−0.022
$\Delta(C_3C_4)$	0.030	0.034	0.038	0.042
$\Delta(C_4C_5)$	−0.039	−0.044	−0.039	−0.043
$\Delta(C_5C_5)$	0.042	0.048	0.051	0.057

TABLE IV. Comparison of changes in C-C-C bond angles in going from neutral polyacetylene to $(C_9H_9)^-$ and $(C_9H_9)^+$. The bond angles for the neutral chain are from near the center of $H(CH)_{32}H$ (122.90° for AM1 calculations and 124.79° for MNDO calculations). The bond angles for $(C_9H_9)^-$ and $(C_9H_9)^+$ are obtained from the bond angles for $[H(CH)_{23}H]^{3-}$ and $[H(CH)_{23}H]^{3+}$, respectively.

	$(C_9H_9)^-$		$(C_9H_9)^+$	
Central carbon	AM1	MNDO	AM1	MNDO
C_1	0.73°	0.69°	−0.28°	−0.12°
C_2	2.86	2.45	−0.58	−0.25
C_3	0.50	0.84	−0.37	−0.18
C_4	2.10	1.79	−0.69	−0.39
C_5	1.07	1.26	−0.50	−0.31

centers-of-symmetry is near unity (i.e., −0.98 for the anion calculations and +0.97 for the cation calculations). These results indicate that the charge distribution and geometries for the $H(CH)_{23}H$ triply charged anions and cations correspond to that for a central soliton located midpoint between two antisolitons. Because of the above mentioned consistency in total charge on chain segments

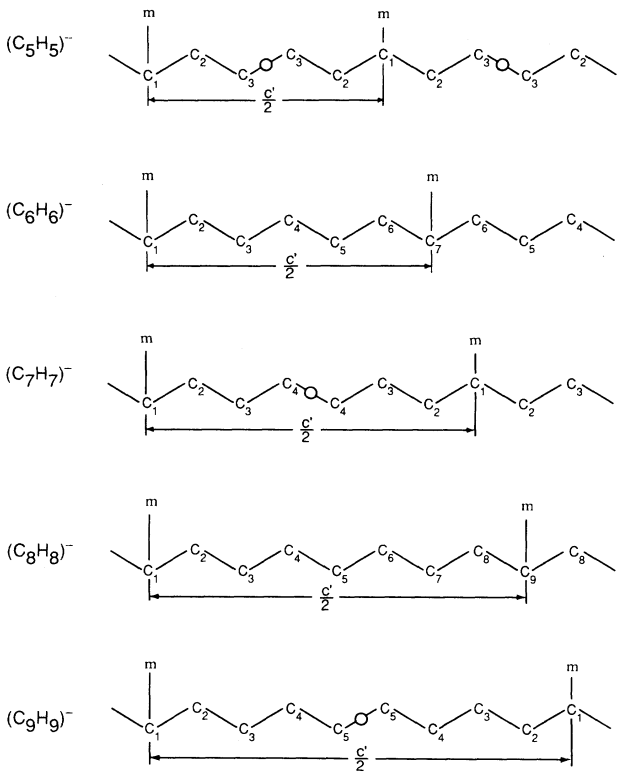

FIG. 4. Mirror planes (m) and centers of symmetry (○), which describe the geometry and charge distribution for investigated soliton lattices, split-soliton lattices, and soliton–split-antisoliton lattices. The length c' corresponds to the lattice repeat length. The carbon numbering indicted here is used in Tables II–VIII. Carbon atoms that share the same index are equivalent for the isolated chain and hydrogen indices are the same as for the corresponding carbons.

and the quasisymmetries, the charges and dimensions on the central part of $H(CH)_{23}H$ triply charged anions and cations provided the charges and geometries for $(C_9H_9)^-$ and $(C_9H_9)^+$ soliton lattices.

The results shown in Table II indicate that the charges calculated on CH groups by AM1 and MNDO are the same within 0.03 electrons. These calculations also indicate that, except for a sign change, the calculated charges on CH units are basically the same for the positive and negative soliton lattices. Similar correspondence between AM1 and MNDO calculations on the same ion and between calculations on anions and cations by either AM1 or MNDO does not result for the charges on carbons, because the amount of charge on hydrogen atoms is significant and is substantially larger for the AM1 calculations than for the MNDO calculations. However, as indicated by the last data line in Table II, even with respect to individual atomic charges there is consistency between the calculated results by AM1 and MNDO on both $(C_9H_9)^-$ and $(C_9H_9)^+$. Specifically, there is little atom-to-atom variation in the charges on hydrogens for the calculated charge distributions for both $(C_9H_9)^-$ and $(C_9H_9)^+$ by either AM1 or MNDO. As shown in Table II, the average change in these hydrogen charges in going from the neutral polymer to other negative or positive soliton lattices has the same absolute value (positive for cation lattices and negative for anion lattices) independent of the sign of the soliton lattice or the calculation method. Consequently, calculated hydrogen charges (or carbon charges) by AM1 and MNDO for the soliton lattices differ by the difference in calculated hydrogen charges for neutral polyacetylene. Using calculated atomic charges in the central part of neutral $H(CH)_{32}H$, these charges on the hydrogens for neutral polyacetylene are 0.125 for AM1 and 0.050 for MNDO. The charges on the carbons in neutral polyacetylene naturally have the same value, but opposite sign. Note that the AM1-calculated carbon charge for neutral polyacetylene is in very good agreement with the carbon charge (-0.134) deduced[45] from the ratio of infrared intensities for bands due to in-plane bending (ν_{HCC}) and C-H stretching (ν_H).

The bond lengths calculated by AM1 and MNDO for either anion or cation soliton lattices differ. However, the differences in the bond lengths calculated by AM1 and MNDO almost precisely correspond to the difference in average carbon-carbon bond length for neutral polyacetylene calculated using these model Hamiltonians. Using the bond lengths in the central part of neutral $H(CH)_{32}H$ to represent those of neutral polyacetylene, carbon single and double bond lengths of 1.444 and 1.347 Å, respectively, are obtained by AM1. The corresponding values obtained by MNDO are 1.462 and 1.358 Å, respectively, and those derived for polyacetylene from x-ray diffraction results on trans, trans-1,3,5,7-octatetraene[46] are 1.451(5) and 1.327(4) Å, respectively. Nuclear magnetic resonance measurements on transpolyacetylene[47,48] result in a single bond length (1.45±0.01 Å) and a double bond length (1.35±0.01 Å) which are in agreement with the above calculated values. As shown in Table III, the calculated changes in bond lengths for the soliton lattices, relative to the average bond length obtained by the same calculation method for neutral polyacetylene, are in excellent agreement for AM1 and MNDO methods. The bond lengths calculated by either AM1 or MNDO are quite similar for $(C_9H_9)^-$ and $(C_9H_9)^+$, but differences of almost 0.01 Å exist in bond lengths calculated by the same method for the anion and cation soliton lattices.

The C-H bond lengths for neutral polyacetylene obtained from AM1 and MNDO calculations of C-H bond lengths in the center of $[H(CH)_{23}H]$ are 1.104 and 1.096 Å, respectively. Using $[H(CH)_{23}H]^{3-}$ and $[H(CH)_{23}H]^{3+}$ as model compounds, the AM1 and MNDO evaluations of $(C_9H_9)^-$ and the MNDO evaluation of $(C_9H_9)^+$ provided average C-H bond lengths in the soliton lattice that are within 0.001 Å of the above calculated values for neutral polyacetylene. In contrast, the average C-H bond length obtained in the same way by AM1 for $(C_9H_9)^+$ is 0.0043 Å larger than the above AM1-calculated value for the C-H bond in neutral polyacetylene. The significant increase in average C-H bond length only for the AM1-calculated $(C_9H_9)^+$ lattice can be understood as an effect due to decreased Coulomb repulsion between calculated charges on carbon, q(C), and on hydrogen, q(H). Specifically, the average change in q(C)q(H) is positive and a factor of 6 or more larger in magnitude for the AM1-calculated $(C_9H_9)^+$ lattice than for the AM1-calculated $(C_9H_9)^-$ lattice or the MNDO-calculated $(C_9H_9)^+$ or $(C_9H_9)^-$ lattices. Nevertheless, the AM1 and MNDO calculations provide nearly the same atom-to-atom variations in C-H bond lengths along the chain in $(C_9H_9)^-$ and in $(C_9H_9)^+$. The individual C-H bond lengths generally increase with decreasing magnitude negative carbon charge relative to the average carbon charge for a specified lattice, which is an aspect that we will later quantify. However, the maximum magnitude deviations between C-H lengths in the $(C_9H_9)^-$ lattice (0.0099 Å by AM1 and 0.0088 Å by MNDO) are significantly larger than for the $(C_9H_9)^+$ lattice (0.0035 Å by AM1 and 0.0028 Å by MNDO).

Table IV indicates a major difference in calculated geometry for the anion and cation soliton lattices for polyacetylene. Large fluctuations in C-C-C bond angles are predicted for $(C_9H_9)^-$, but not for $(C_9H_9)^+$. The C-C-C bond angle calculated by AM1 (using the geometry in the center of neutral $H(CH)_{32}H$) for neutral polyacetylene is smaller (122.90°) than that obtained by MNDO (124.79°) and that experimentally derived[47] for polyacetylene from the structure of $H(CH)_8H$ [125.3(4)°]. However, Table IV shows that there is good agreement between the AM1 and MNDO calculated changes in this bond angle upon formation of the soliton lattice. Also, the C-C-C bond angle derived by AM1 for polyacetylene is close to the value (120.7±1.5°) obtained[47] from ^{13}C two-dimensional NMR combined with dynamic nuclear polarization.

Table V shows the calculated differences in H-C-C bond angles to the same central carbon for the $(C_9H_9)^-$ and $(C_9H_9)^+$ soliton lattices. The AM1 and MNDO calculations provide almost identical results. However, while the calculated deviations are similar for corresponding angles in $(C_9H_9)^-$ and in $(C_9H_9)^+$, they are

TABLE V. Deviation between H-C-C bond angles to the same central carbon. Calculated results using AM1 and MNDO utilize the geometry of $[H(CH)_{23}H]^{3-}$ and $[H(CH)_{23}H]^{3+}$ to obtain bond angles for $(C_9H_9)^-$ and $(C_9H_9)^+$, respectively. Deviations are defined to be positive when the largest bond angle involves the shortest C-C bond to a specified carbon.

	$(C_9H_9)^-$		$(C_9H_9)^+$	
Central carbon	AM1	MNDO	AM1	MNDO
C_1	0°	0°	0°	0°
C_2	0.93	0.96	1.41	1.42
C_3	2.33	2.41	2.54	2.45
C_4	2.51	2.59	3.56	3.51
C_5	3.34	3.32	4.16	4.06

somewhat larger in some instances for $(C_9H_9)^+$. Using the central part of $H(CH)_{32}H$ to obtain angles for neutral polyacetylene, the difference in H-C-C bond angles to the same carbon for neutral polyacetylene is 4.20° by AM1 (angles of 120.65° and 116.45°) and 3.93° by MNDO (angles of 119.56° and 115.63°). The calculated angle between the C-H bond and the chain-axis direction deviates slightly from 90° for both AM1 (91.02°) and MNDO calculations (90.84°) for neutral polyacetylene.

The agreement between charge distribution and geometry derived for soliton lattices using calculated parameters for different length polyenes indicates the absence of significant chain-end effects on the parameters derived for a specified soliton lattice. For example, $[H(CH)_{23}H]^{3-}$ contains a soliton on the central carbon and one antisoliton on either side of this center, with a soliton-antisoliton spacing of nine carbon atoms. In contrast, $[H(CH)_{32}H]^{4-}$ contains a soliton and an antisoliton equivalently located on opposite sides of the molecular center, also with a soliton-antisoliton spacing of nine carbon atoms. In both cases, parameters for the soliton lattice were calculated by averaging the nearly equal parameter values on either side of the innermost soliton. The resulting carbon charges, charges on CH units, C-C bond lengths, and C-C-C bond angles derived for $(C_9H_9)^-$ using MNDO results for these anions differ at most by 0.003 electron, 0.002 electron, 0.001 Å, and 0.41°, respectively.

Figures 5 and 6 show graphically the variation in carbon charge and chain geometry as a function of chain site in the $(C_9H_9)^-$ and $(C_9H_9)^+$ soliton lattices. The translational period in both cases contains 18 CH units and two charges. However, since the chain symmetry elements are centers of symmetry midway between mirror planes orthogonal to the chain-axis direction, the geometry of the carbon backbone is completely specified by five C-C bond lengths and five C-C-C bond angles, which are provided in Table VI. The differential carbon charge distribution for $(C_9H_9)^+$ is almost the mirror image of that for $(C_9H_9)^-$, in the sense that the deviation of carbon charge from the mean carbon charge (-0.056 and -0.192 for the cation and anion lattices, respectively, by AM1) have nearly the same magnitude for corresponding carbons,

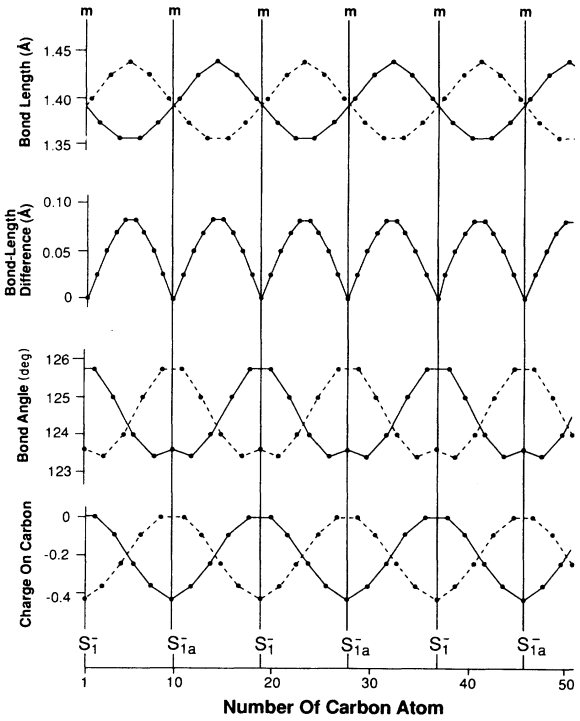

FIG. 5. Geometrical parameters and charge as a function of carbon index (shown in Fig. 4) for the $(C_9H_9)^-$ soliton lattice calculated by AM1. The bond-length difference for carbon C_i is the absolute magnitude of the difference in carbon-carbon bond lengths to this carbon. The dashed and solid lines connect data points for even-index and odd-index carbons, respectively. The location of soliton centers (S_1^-) and antisoliton centers (S_{1a}^-) are indicated.

but the signs of these deviations are reversed in going from the cation to the anion. Also, bond lengths for corresponding bonds in $(C_9H_9)^+$ and $(C_9H_9)^-$ are comparable. Every other bond has a decreased length relative to the neighboring bonds in the region between two mirror planes. The length of these shortened bonds is almost precisely the same for $(C_9H_9)^+$ and $(C_9H_9)^-$, but the elongated bonds are somewhat longer for the cation than for the anion (by from 0.007 to 0.009 Å). In contrast with the above similarities, Figs. 5 and 6 also depict the dramatically different C-C-C bond angles variations for the anion and cation soliton lattices.

Parameters for the $(C_9H_9)^-$, $(C_7H_7)^-$, and $(C_5H_5)^-$ soliton lattice are compared in Table VI. These parameters for $(C_7H_7)^-$ were obtained from AM1 calculations $[H(CH)_{32}H]^{6-}$. The charge and bond-length distributions in the central part of this anion are consistent with the presence of both a soliton and an antisoliton on either side of the anion center, which have a separation of seven CH units between soliton and antisoliton. The parameters shown in Table VI were obtained by averaging the nearly equal values calculated on opposite sides of the anion center. The sum of calculated charges per $(C_7H_7)^-$ unit equals 1.09 electron, whose deviation from unity reflects the approximations in deriving soliton lattice charges from the oligomer anion calculation. For com-

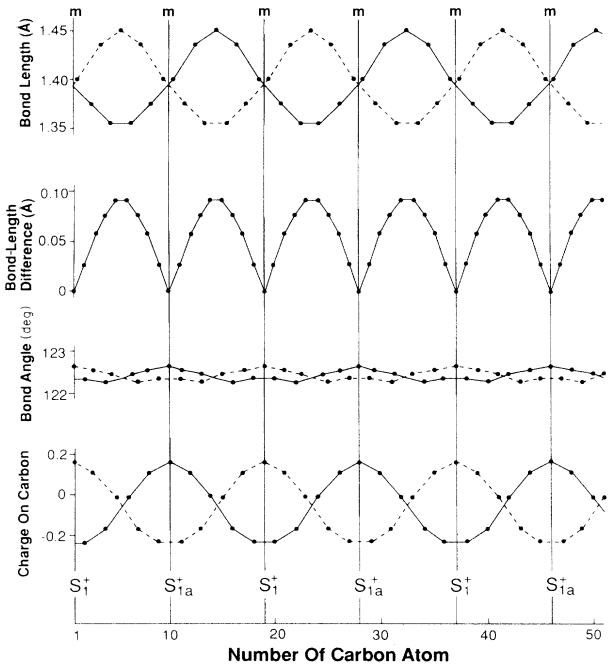

FIG. 6. Geometrical parameters and charge as a function of carbon index (shown in Fig. 4) for the $(C_9H_9)^+$ soliton lattice calculated by AM1. The bond-length difference for carbon C_i is the absolute magnitude of the difference in carbon-carbon bond lengths to this carbon. The dashed and solid lines connect data points for even-index and odd-index carbons, respectively. The location of soliton centers (S_1^+) and antisoliton centers (S_{1a}^+) are indicated.

parison with the results in Table VI, parameters for the $(C_7H_7)^-$ soliton lattice were also derived from AM1 calculations on $[H(CH)_{39}H]^{7-}$. The charge and bond-length distributions for the central part of this anion can be represented by a central soliton, which is surrounded on both sides by antisolitons, so that the soliton-antisoliton spacing is seven CH units. Geometry and charge distribution were obtained by averaging parameters calculated for the region between the central soliton and a neighboring antisoliton. The thereby derived total charge on the soliton was 1.065 electrons, whose deviation from unity again corresponds to calculation error due to the use of oligomer charges to derive charges for the polymer soliton lattice. The differences between AM1 calculated parameters for $(C_7H_7)^-$ using $[H(CH)_{39}H]^{7-}$ and $[H(CH)_{32}H]^{6-}$ were small. The maximum magnitude difference in carbon charges, CH charges, C-C bond lengths, and C-C-C bond angles using these two polyene oligomers were 0.0074 electron, 0.0085 electron, 0.001 Å, and 0.11°, respectively.

The parameters associated with the $(C_5H_5)^-$ soliton lattice were derived from AM1 calculations on $[H(CH)_{16}H]^{4-}$. The carbon charges and quasisymmetries of this anion are consistent with a soliton and antisoliton symmetrically located with respect to the molecular center. Averaging the nearly equal calculated charges and dimensions about the anion center provides the results shown in Table VI for the $(C_5H_5)^-$ soliton lattice. This anion is apparently a very good model for $(C_5H_5)^-$, since the total CH charge derived for $(C_5H_5)^-$ from the charges on the oligomer anion (0.987 electron) is very close to unity.

TABLE VI. Summary of calculated parameters for the odd-carbon soliton lattices $(C_9H_9)^-$, $(C_7H_7)^-$, and $(C_5H_5)^-$. Structural diagrams showing atom labeling are provided in Fig. 4. The solitons and antisolitons are centered at C_1 carbons. The tabulated parameters for $(C_9H_9)^-$, $(C_7H_7)^-$, and $(C_5H_5)^-$ resulted from AM1 calculations on $[H(CH)_{23}H]^{3-}$, $[H(CH)_{32}H]^{6-}$, and $[H(CH)_{16}H]^{4-}$, respectively.

		(C_9H_9)	
Charge on carbon	Charge on CH	Bond length (Å)	C-C-C Bond angle (deg)[a]
C_1 −0.421	C_1H_1 −0.327	C_1C_2 1.398	C_1 123.63
C_2 0.012	C_2H_2 0.078	C_2C_3 1.373	C_2 125.76
C_3 −0.364	C_3H_3 −0.271	C_3C_4 1.425	C_3 123.40
C_4 −0.069	C_4H_4 0.009	C_4C_5 1.356	C_4 125.00
C_5 −0.231	C_5H_5 −0.142	C_5C_5 1.438	C_5 123.97
		$(C_7H_7)^-$	
Charge on carbon	Charge on CH	Bond length (Å)	C-C-C Bond angle (deg)[a]
C_1 −0.463	C_1H_1 −0.389	C_1C_2 1.399	C_1 124.04
C_2 −0.006	C_2H_2 0.044	C_2C_3 1.374	C_2 126.72
C_3 −0.377	C_3H_3 −0.304	C_3C_4 1.435	C_3 124.37
C_4 −0.155	C_4H_4 −0.091	C_4C_4 1.358	C_4 125.48
		$(C_5H_5)^-$	
Charge on carbon	Charge on CH	Bond length (Å)	C-C-C Bond angle (deg)[a]
C_1 −0.502	C_1H_1 −0.445	C_1C_2 1.410	C_1 124.28
C_2 −0.052	C_2H_2 −0.013	C_2C_3 1.367	C_2 127.05
C_3 −0.312	C_3H_3 −0.258	C_3C_3 1.441	C_3 125.19

[a]The central carbon in each C-C-C bond angle is specified.

D. Even-carbon soliton–split-antisoliton lattices

We next consider the situation where the number of carbons per added electron is an even number. This case is more complicated than the case where the number of carbons per electron is odd, since the separation between conventional solitons and antisolitons must correspond to an odd number of carbons. For example, a soliton lattice with one charge per six carbons could be described by a periodic 5-7 sequence of solitons and antisolitons in which successive soliton-antisoliton separations alternate between five carbons and seven carbons, as illustrated in Fig. 7. Such sequences in which alternate solitons are separated by different odd numbers of carbon atoms is not seen in the charge distributions of the model compounds. Instead, an observed sequence for the model compounds corresponds to the alternation of solitons and split antisolitons (or, equivalently, antisolitons and split solitons), which is shown at the bottom of Fig. 7. The resulting symmetry of charge distribution and molecular dimensions is represented in Fig. 4 for the $(C_6H_6)^-$ and $(C_8H_8)^-$ soliton lattices.

The first example of such soliton–split-antisoliton sequences was noted for $[H(CH)_{25}H]^{5-}$. The charge distribution for this anion is consistent with the existence of a soliton at the anion center, which is surrounded on both sides by split antisolitons, providing a separation between the soliton and split antisolitons of six CH units. Local charge distribution and anion geometry indicate a quasimirror plane or mirror plane through the centers of both the solitons and split antisolitons. Mirror planes are indicated in these positions in the molecular model for $(C_6H_6)^-$, which is shown in Fig. 4.

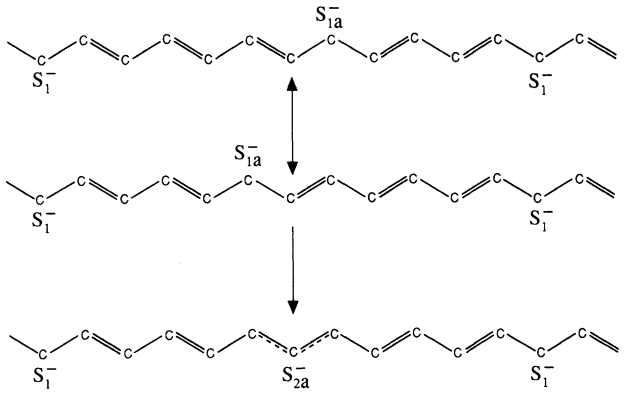

FIG. 7. The bottom chain shows the array of solitons (S_1^-) and split antisolitons (S_{2a}^-) that best represents the geometry and charge distribution for $(C_6H_6)^-$. While an array of solitons and antisolitons (top two chains) has higher energy, the geometry and charge distribution for the soliton–split-antisoliton array on the bottom chain is well approximated as an average of that for the top two chains in the figure, which differ only in a relative chain-axis displacement of two CH units.

The AM1-derived charge distribution and geometry dimensions provided in Table VII for $(C_6H_6)^-$ resulted from averaging the nearly equal calculated parameters on either side of the central soliton for $[H(CH)_{25}H]^{5-}$. The suitability of the model anion for deriving parameters for $(C_6H_6)^-$ is suggested by the near unity value (0.989 elec-

TABLE VII. Summary of calculated parameters for the even-carbon lattices $(C_8H_8)^-$ and $(C_6H_6)^-$. Structural diagrams showing atom labeling are provided in Fig. 4. The solitons are centered on the C_1 carbon and the split antisolitons are centered on the highest index carbon. The tabulated parameters for $(C_8H_8)^-$ and $(C_6H_6)^-$ resulted from AM1 calculations on $[H(CH)_{33}H]^{5-}$ and $[H(CH)_{25}H]^{5-}$, respectively.

		$(C_8H_8)^-$	
Charge on carbon	Charge on CH	Bond length (Å)	C-C-C Bond angle (deg)[a]
C_1 −0.440	C_1H_1 −0.353	C_1C_2 1.402	C_1 123.62
C_2 0.001	C_2H_2 0.061	C_2C_3 1.371	C_1 126.08
C_3 −0.361	C_3H_3 −0.276	C_3C_4 1.431	C_3 124.05
C_4 −0.112	C_4H_4 −0.037	C_4C_5 1.355	C_4 125.05
C_5 −0.188	C_5H_5 −0.109	C_5C_6 1.438	C_5 124.75
C_6 −0.290	C_6H_6 −0.207	C_6C_7 1.362	C_6 124.03
C_7 −0.036	C_7H_7 0.028	C_7C_8 1.416	C_7 125.85
C_8 −0.429	C_8H_8 −0.344	C_8C_9 1.388	C_8 123.59
C_9 0.015	C_9H_9 0.071		C_9 126.31
		$(C_6H_6)^-$	
Charge on carbon	Charge on CH	Bond length (Å)	C-C-C Bond angle (deg)[a]
C_1 −0.471	C_1H_1 −0.399	C_1C_2 1.406	C_1 124.22
C_2 −0.022	C_2H_2 0.026	C_2C_3 1.369	C_2 126.60
C_3 −0.344	C_3H_3 −0.275	C_3C_4 1.438	C_3 124.64
C_4 −0.210	C_4H_4 −0.146	C_4C_5 1.359	C_4 125.22
C_5 −0.108	C_5H_5 −0.052	C_5C_6 1.427	C_5 126.07
C_6 −0.435	C_6H_6 −0.365	C_6C_7 1.384	C_6 124.16
C_7 0.002	C_7H_7 0.046		C_7 126.97

[a]The central carbon in each C-C-C bond is specified.

tron) of the sum of charges resulting from the averaging. Also, these parameters are consistent with those obtained using MNDO, in the same sense as discussed for the evaluations of $(C_9H_9)^-$ by AM1 and MNDO. Specifically, the maximum deviation between AM1- and MNDO-calculated charge on the CH units is 0.023 electron. After subtraction of the differences in AM1- and MNDO-calculated charge on carbon, average C-C bond length, and C-C-C bond angle for neutral polyacetylene, the maximum deviation between AM1- and MNDO-calculated carbon charge, C-C bond length, and C-C-C bond angle are, respectively 0.028 electron, 0.004 Å, and 0.39°, respectively.

The reliability of the parameters derived for $(C_6H_6)^-$ was also checked by comparing these parameters with those derived from AM1 calculations on $[H(CH)_{32}H]^{6-}$. This anion is less suitable than $[H(CH)_{25}H]^{5-}$ for such analysis, since the 6− anion contains a soliton and an antisoliton symmetrically located about the molecular center, each of which is followed by a split antisoliton (or split soliton). The soliton-antisoliton separation is seven CH units and the separation between solitons and split antisolitons is six CH units. Despite the absence an uninterrupted sequence of more than one soliton and one split antisoliton for $[H(CH)_{32}H]^{6-}$, the parameters derived for $(C_6H_6)^-$ using this anion are in good agreement with those calculated using $[H(CH)_{25}H]^{5-}$ as the model anion. Specifically, the maximum differences between calculated carbon charges, CH charges, C-C bond lengths, and C-C-C bond angles are 0.029 electron, 0.030 electron, 0.0055 Å, and 0.20°, respectively. Also, the total CH charge derived for the polymer −1 anion length using the molecular anion charges (−0.967) is close to unity.

The $(C_6H_6)^-$ array is particularly important in that the corresponding dopant level ($y=0.167$) is close to the limiting doping level for alkali metals in polyacetylene—at least at atmospheric pressure. Several features are evident from the parameters shown in Table VII. First, large site-to-site variations in carbon charges, C-C bond lengths, and C-C-C bond angles are present even at this high doping level. As expected, the carbon-carbon bonds about the soliton centers (C_1-C_2) are longer than those about the centers of the split antisolitons (C_6-C_7). However, neither bond length is either the maximum or minimum length carbon-carbon bond in the $(C_6H_6)^-$ lattice. Second, soliton–split-antisoliton arrays of this type have an inherent asymmetry even in chain-axis projection—since even-carbon and odd-carbon sides of the chain are not equivalent. Nevertheless, the difference in the amount of charge on the two sides of the chain is small. Using the charges in Table VII, this difference in carbon charge is 1.4% of the total excess carbon charge and this difference in CH charge is 1.9% of the total excess CH charge. Both AM1 and MNDO calculations provide almost precisely the same differences in total charge on opposite sides of the backbone (0.0031–0.0035 electron, per carbon or per CH, higher negative charge on the soliton side of the chain than on the opposite side, according to either AM1 or MNDO calculations on $[H(CH)_{25}H]^{5-}$). However, these differences are probably comparable with calculation uncertainties. Consequently, the noteworthy point is that the existence of differing charge distributions for even carbons and for odd carbons results in a near zero difference in average charge on carbons and on CH units on opposite sides of the chain for $(C_6H_6)^-$.

Two separate evaluations of both charge distribution and geometry were obtained for $(C_8H_8)^-$ using AM1 calculations on $[H(CH)_{33}H]^{5-}$ and $[H(CH)_{35}H]^{5-}$. As shown in Fig. 8, the former molecular anion consists of a soliton at the anion center that is surrounded on both sides by split antisolitons. As also illustrated in Fig. 8, the latter anion consists of a split antisoliton at the anion center which is surrounded on both sides by solitons. In both anions the separation between the charge centers is eight CH units. Since the number of carbons per unit charge is even in $(C_8H_8)^-$, this lattice is analogous to that for $(C_6H_6)^-$ in that the structure cannot be described by a sequence of equally spaced solitons and antisolitons. As for the case of $(C_6H_6)^-$, calculations on the model compounds indicate that the $(C_8H_8)^-$ structure corresponds to alternating solitons and split antisolitons. The charge distribution and geometry derived for $(C_8H_8)^-$ from the AM1 calculations on $[H(CH)_{33}H)]^{5-}$ are provided in Table VII. The $[H(CH)_{33}H]^{5-}$ anion was used to derive the parameters in this table, since the total lattice charge obtained from this anion (−1.025) for the C_8H_8 unit in the polymer is very close to unity (versus −0.965 for the corresponding total charge for $(C_8H_8)^-$ derived using $[H(CH)_{35}H]^{5-}$). However, the maximum discrepancies between calculated carbon charges, CH charges, C-C bond distances, and C-C-C bond angles for the two molecular anions are only 0.019 electron, 0.021 electron, 0.0036 Å, and 0.22°.

Note that only p C-C-C bond angles are required to describe the $(C_pH_p)^-$ soliton–split-antisoliton lattices when p is even, since there are mirror planes orthogonal to the chain-axis direction at both the soliton and the split-antisoliton carbon centers. Because of this symmetry, the following relationship exists between the bond angles α_k centered at carbons C_k:

$$(\alpha_1+\alpha_2)/2+\sum_{k=2}^{p+1}\alpha_k=0\ . \tag{2}$$

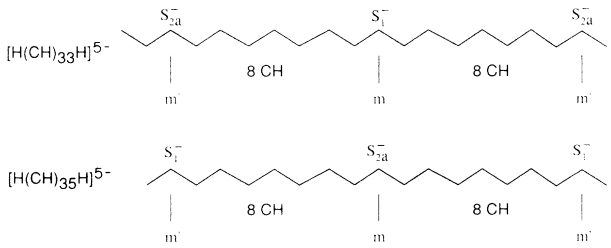

FIG. 8. The array of solitons (S_1^-) and split antisolitons (S_{2a}^-) indicated by the observed charge distribution and geometry for $[H(CH)_{33}H]^{5-}$ and $[H(CH)_{35}H]^{5-}$, which are model anions for the $(C_8H_8)^-$ lattice. Mirror planes (m) and approximate mirror planes (m') are indicated for these oligomers.

Substitution of the $p+1$ bond angles provided by the geometry of the molecular anions (Table VII) into the left-hand side of Eq. (2) results in a value of 0.33° for the $(C_6H_6)^-$ evaluation and 0.87° for the $(C_8H_8)^-$ evaluation. The deviations of these numbers from zero represent errors resulting from the approximation of polymer anion geometry by molecular anion geometry. Such errors can be approximately corrected for by changing the individual bond angles in Table VII by $(-1)^k(0.054°)$ for $(C_6H_6)^-$ and by $(-1)^k(0.018°)$ for $(C_8H_8)^-$.

The charges and geometrical parameters for the $(C_8H_8)^-$ lattice are presented graphically in Fig. 9. This lattice is especially interesting because of the highly symmetric structure which would be feasible for the corresponding $(C_4H_4)_2M$ phase in the absence of the charge and structural oscillations that are derived herein. Also, as we discussed in Sec. II, diffraction data is available for $(C_4H_4)_2K$, which suggests the alkali-metal column and polymer-chain periodicities are commensurate. This diffraction data is consistent with a chain-axis repeat length of four CH units, but is also consistent with the longer repeat length suggested by the present theory (16 CH units), since the effect of the longer periodicity on meridional diffraction intensities would be difficult to detect. The charge oscillations for the investigated soliton lattices and soliton–split-antisoliton lattices are compared in Fig. 10.

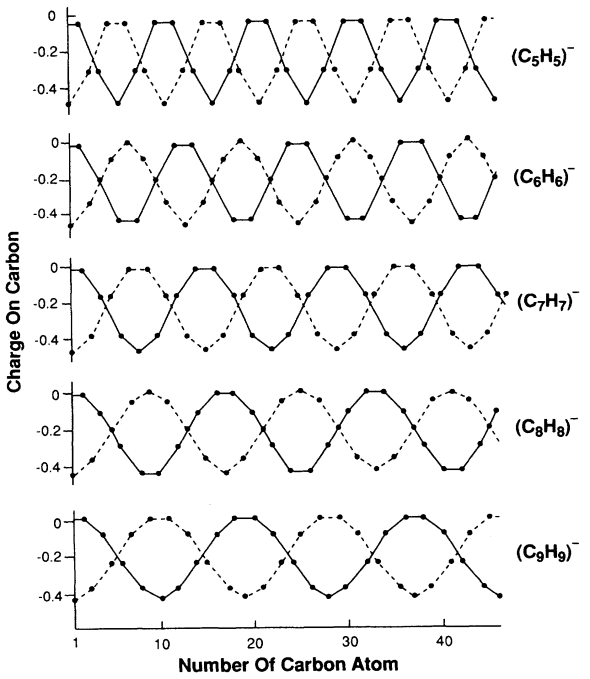

FIG. 10. Comparison of AM1-calculated charge oscillations for $(C_pH_p)^-$ soliton lattice (p even) and soliton–split-antisoliton lattices (p odd). The dashed and solid lines connect data points for even-index and odd-index carbons, respectively.

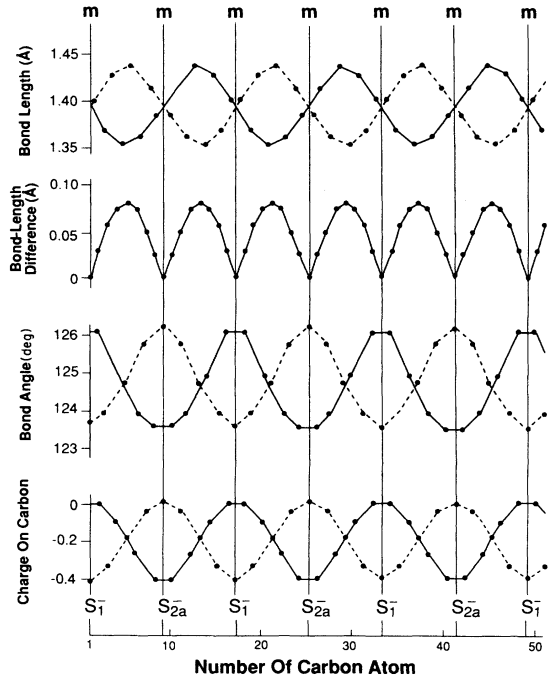

FIG. 9. Geometrical parameters and charge as a function of carbon index (shown in Fig. 4) for the $(C_8H_8)^-$ soliton–split-antisoliton lattice calculated by AM1. The bond-length difference for carbon C_i is the absolute magnitude of the difference in carbon-carbon bond lengths to this carbon. The dashed and solid lines connect data points for even-index and odd-index carbons, respectively. The location of soliton centers (S_1^-) and split-antisoliton centers (S_{2a}^-) are indicated.

Note that the AM1 calculations on $(C_8H_8)^-$ provide a lower total charge on carbons on the soliton side of the chain as compared to that for the carbons on the opposite side of the chain. From the charges for $(C_8H_8)^-$ derived using AM1 results for $[H(CH)_{33}H]^{5-}$, the carbons on the soliton side of the chain are less negative than those on opposite side of the chain by an average of 0.0040 electrons/carbon. The corresponding difference in $[H(CH)_{35}H]^{5-}$ derived average carbon charge for these two sides of the chain is almost twice as large (0.0075 electrons/ carbon), suggesting again that the charge imbalance for the carbons on the two sides of the chain is too small for reliable evaluation by the present analyses.

Figure 11 shows the oscillations in local chain-axis direction for the $(C_8H_8)^-$ soliton–split-antisoliton lattice, which is obtained using the parameters from Table VII. Carbon atom deviations from the average chain-axis direction are magnified ten-fold relative to the scale for coordinates in the average chain-axis direction, in order to clearly illustrate the oscillations in local chain-axis direction. As for the other lattices investigated, carbons having the most negative charge have the largest deviations from the lateral center of mass of the chain, while those having more positive charge are located closer to this center of mass. As we will discuss in Sec. IV and as shown in Fig. 11, the result of such oscillations in local chain-axis direction is to bring the most negatively charged carbons on one side of the chain closer to the offset position of the column of alkali-metal ion columns that is derived from experimental results.[8,12,13]

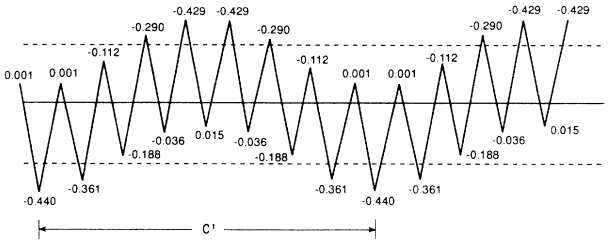

FIG. 11. Illustration of oscillation in local chain direction for the $(C_8H_8)^-$ soliton–split-antisoliton lattice. Chain carbon coordinates are represented using a ten-fold higher magnification for the vertical axis (orthogonal to average chain direction) relative to that for the horizontal axis (average chain direction). The numbers indicated are carbon charges derived from AM1 calculations. The solid horizontal line corresponds to the average chain center and the dashed lines correspond to alternate locations for the ion column according to the model of Chen *et al.* (Ref. 13).

E. Odd-carbon split-soliton lattices

Depending upon the length of the model polyene and the number of charges, the derived geometry and charge distribution for $(C_9H_9)^-$ and $(C_7H_7)^-$ arrays corresponds to a soliton lattice or a split-soliton lattice. In both cases the translational period corresponds to two such units, which are related by a bond-centered center of symmetry. Also, in both cases, mirror planes orthogonal to the chain are located midway between these centers of symmetry. This mirror plane is the center of the soliton for the soliton lattice and the center of the split soliton for the split-soliton lattice, as shown in Fig. 12, where bond lengths and carbon charge variations are compared for the $(C_7H_7)^-$ soliton and split-soliton lattices and for the $(C_8H_8)^-$ soliton–split-antisoliton lattice. The principal difference is that these mirror planes coincide with carbons having maximum charge for the soliton lattice and with carbons having near zero charge for the split-soliton lattice. In the latter case, maximum charge is on the two carbons bound to the carbon that is on the mirror plane.

We have earlier in this section derived (1) the soliton lattice for $(C_9H_9)^-$ from the calculated structures for $[H(CH)_{23}H]^{3-}$ and $[H(CH)_{32}H]^{4-}$ and (2) the soliton lattice for $(C_7H_7)^-$ from the calculated structures for $[H(CH)_{32}H]^{6-}$ and $[H(CH)_{32}H]^{7-}$. Independent of the model chosen, the derived soliton charges and geometries are in exceptional agreement. In contrast, the calculated charges and geometries of $[H(CH)_{39}H]^{5-}$ and $[H(CH)_{41}H]^{7-}$ are incompatible with soliton representations, but are fully consistent with split-soliton representations. Using these anion models we will derive the split-soliton lattices for $(C_9H_9)^-$ and $(C_7H_7)^-$, respectively. The representation of the model anions for the $(C_7H_7)^-$ soliton lattices and the split-soliton lattices in terms of solitons (S_1), antisolitons (S_{1a}), split solitons (S_2), and split antisolitons (S_{2a}) is shown in Fig. 13.

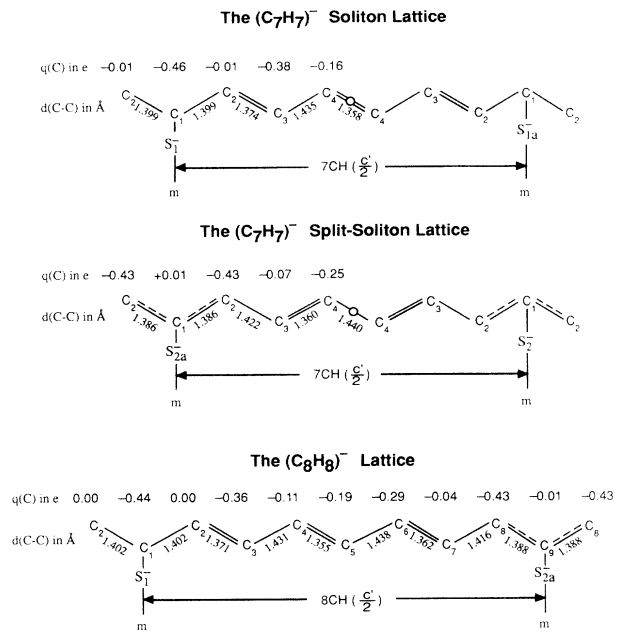

FIG. 12. Comparison of bond-length and carbon charge variations for the $(C_7H_7)^-$ soliton and split-soliton lattices and for the $(C_8H_8)^-$ soliton–split-antisoliton lattice. Mirror planes (m) are indicated, as is one-half the lattice periodicity ($c'/2$).

The present observations that the calculated geometry and charge distribution switches between soliton array and split-soliton array with changes in monomer length and charge is not surprising in light of the theoretical work of Takahashi and Fukutome.[43] These authors used a Pariser-Parr-Pople type model (which is an extended Hubbard Hamiltonian supplemented by a σ-bond compressibility term within the spin unrestricted

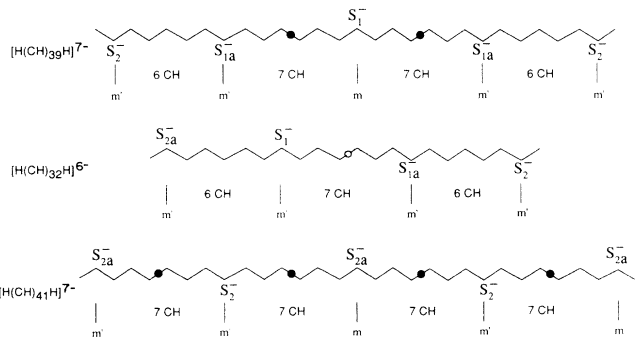

FIG. 13. The arrangement of solitons (S_1), antisolitons (S_{1a}), split solitons (S_2), and split antisolitons (S_{2a}) which generates the observed geometry and charge distribution for oligomeric anions used for models for the $(C_7H_7)^-$ soliton lattice and split-soliton lattice. Mirror planes (m), approximate mirror planes (m'), centers of symmetry (○) and approximate centers of symmetry (●) are indicated, as is the separation between charge centers.

Hartree-Fock approximation) to calculate geometry, charge distribution, and total energy of an equally spaced charged soliton and charged antisoliton pair in a lattice with 62 carbons and periodic boundary conditions. They obtained almost precisely the same total energy for this calculation as for the calculation in which the charged soliton and charged antisoliton pair was replaced by a charged split-soliton and a charged split-antisoliton pair.

The results obtained for charge distribution and geometry for the split-soliton lattices of $(C_9H_9)^-$ and $(C_7H_7)^-$ are provided in Table VIII. Also, the charge distribution and geometry for the $(C_9H_9)^-$ split-soliton lattice are shown graphically in Fig. 14. The model anions used to obtain these results contain a split soliton at chain center and a total of either three or five split solitons, which are well separated from the chain ends. Charge distribution and molecular geometry was derived by averaging nearly equal calculated parameters obtained on opposite sides of the split soliton at chain center. The charges obtained from the oligomer results sum to -0.969 for the $(C_9H_9)^-$ split-soliton lattice and -1.005 for the $(C_7H_7)^-$ split-soliton lattice, indicating the consistency of the analyses.

F. Lattices with noninteger numbers of CH units per unit charge

It is interesting to determine the soliton lattice charge distribution that is expected when the average number of CH units per unit charge is noninteger. The oligomer anion calculations again provide useful insights. The charge distribution and geometry associated with the x-2 inner charges for the $[H(CH)_uH]^{x-}$ anions can be fully described by arrays involving various combinations of solitons, antisolitons, split solitons, and split antisolitons. The separations between neighboring charge centers define segment lengths that are either all equal or are v CH units for inner pairs and $v-1$ CH units for the two outer pairs on opposite ends of the molecule, where v is a positive integer. Such AM1-observed arrangements are quite reasonable, since minimization of the difference in the average charge density (per CH) on adjacent chain segments is expected to minimize electrostatic energy.

Based on the results for the oligomer anions, we can anticipate the form of the anion lattice which has on average one electron excess charge per $p+\delta$ CH units,

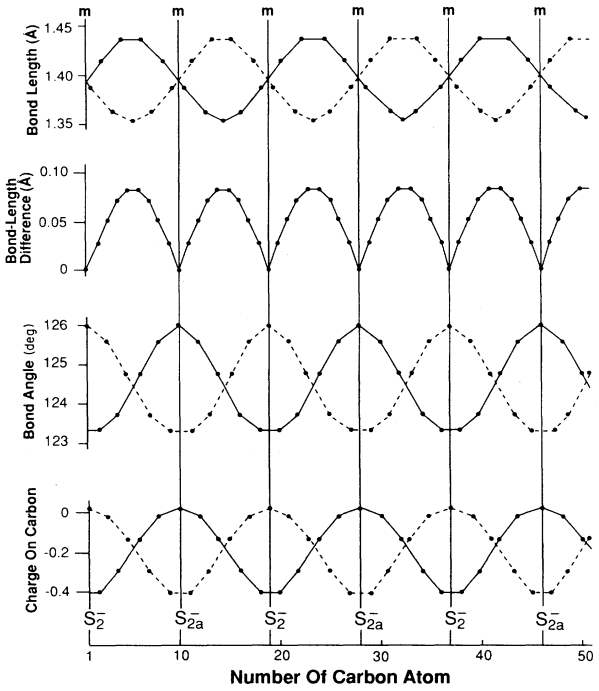

FIG. 14. Geometrical parameters and charge as a function of carbon index (shown in Fig. 4) for the $(C_9H_9)^-$ split-soliton lattice calculated by AM1. The bond-length difference for carbon C_i is the absolute magnitude of the difference in carbon-carbon bond lengths to this carbon. The dashed and solid lines connect data points for even-index and odd-index carbons, respectively. The location of split-soliton centers (S_2^-) and split-antisoliton centers (S_{2a}^-) are indicated.

TABLE VIII. Summary of calculated parameters for the odd-carbon split-soliton lattices $(C_9H_9)^-$ and $(C_7H_7)^-$. Structural diagrams showing atom labeling are provided in Fig. 4. The split solitons and split antisolitons are centered on C_1 carbons. The tabulated parameters for $(C_9H_9)^-$ and $(C_7H_7)^-$ resulted from AM1 calculations on $[H(CH)_{39}H]^{5-}$ and $[H(CH)_{41}H]^{7-}$, respectively.

		$(C_9H_9)^-$	
Charge on carbon	Charge on CH	Bond length (Å)	C-C-C Bond angle (deg)[a]
C_1 0.022	C_1H_1 0.085	C_1C_2 1.385	C_1 125.98
C_2 −0.408	C_2H_2 −0.314	C_2C_3 1.414	C_2 123.37
C_3 −0.021	C_3H_3 0.049	C_3C_4 1.362	C_3 125.57
C_4 −0.301	C_4H_4 −0.209	C_4C_5 1.436	C_4 123.68
C_5 −0.137	C_5H_5 −0.053	C_5H_5 1.353	C_5 124.70
		$(C_7H_7)^-$	
Charge on carbon	Charge on CH	Bond length (Å)	C-C-C Bond angle (deg)[a]
C_1 0.011	C_1H_1 0.063	C_1C_2 1.386	C_1 126.52
C_2 −0.428	C_2H_2 −0.349	C_2C_3 1.422	C_2 124.02
C_3 −0.067	C_3H_3 −0.006	C_3C_4 1.360	C_3 126.07
C_4 −0.253	C_4H_4 −0.179	C_4C_4 1.440	C_4 124.87

[a]The central carbon in each C-C-C bond is specified.

where δ is less than unity. The anion lattice expected in this case contains a mixture of a fraction δ of segments containing $p+1$ CH units and a fraction $1-\delta$ of segments containing p CH units. From the oligomer anion results, the odd length segments must consist of either segments between solitons and antisolitons or between split solitons and split antisolitons. Similarly, the segments containing even numbers of CH units must be limited on opposite ends by solitons and split antisolitons or antisolitons and split solitons.

These results from oligomer calculations also indicate that the charge distribution and geometry of these differing segments are insensitive to the nature of the adjacent segments. Hence, the charge distribution and geometries in Tables VI–VII can be used to construct the charge distributions and geometries for lattices in which the average number of CH units per unit charge is noninteger. Specific evidence for such transferability is the good agreement between the carbon charges, C-C bond lengths, and C-C-C bond angles for the split-antisoliton, soliton, antisoliton, soliton, and split-antisoliton array observed in the AM1 calculations on $[H(CH)_{39}H]^{7-}$ and those obtained using the Table VI and VII results for the following array: $(C_6H_6)^-(C_7H_7)^-(C_7H_7)^-(C_6H_6)^-$. The maximum discrepancies between the results of direct AM1 calculation on the model anion and the results obtained using Tables VI and VII are 0.029 for carbon charge, 0.006 Å for bond distance, and 0.22° for C-C-C bond angle.

The way in which anion segments of different length, each with $1-$ charge, would assemble in a chain is a complicated issue. Consider first a low fraction of odd length segments in a sequence of even length segments. An example would be a small number of isolated $(C_7H_7)^-$ segments in a $(C_8H_8)^-$ array. Such $(C_7H_7)^-$ segments could be randomly located between $(C_8H_8)^-$ segments, but one-half of such randomly located $(C_7H_7)^-$ would then have the soliton-antisoliton configuration and one-half would have the split-soliton–split-antisoliton configuration. Which configuration results depends upon whether the adjacent end of a $(C_8H_8)^-$ segment is the soliton end (or antisoliton end) or the split-antisoliton end (or split-soliton end) of such a segment. Likewise, a single $(C_8H_8)^-$ segment in a $(C_7H_7)^-$ array would change a soliton-antisoliton configuration for the $(C_7H_7)^-$ segments on the right of the $(C_8H_8)^-$ segment to a split-soliton–split-antisoliton configuration for the $(C_7H_7)^-$ on the left of the $(C_8H_8)^-$ segment. Only if an even number of $(C_8H_8)^-$ segments are aggregated together would the configuration of the $(C_7H_7)^-$ segments on the left and the right of these $(C_8H_8)^-$ segments be equivalent. The extent to which random mixing of segments occurs at a particular temperature depends upon the entropy of this mixing compared with the enthalpy change associated with aggregation of like segments. In the concentration limit where both odd and even segments have comparable concentrations, one can describe various periodic structures. An interesting structure of this type corresponds to alternating even-carbon segments and odd-carbon segments, the latter alternating between soliton-antisoliton and split-soliton–split-antisoliton configurations.

Such anion structures with noninteger numbers of carbons per unit charge can be important from several viewpoints. First, such structures with low concentration of the minority sequence could arise because of vacancies or interstitials in the ion columns. More generally, such structures could arise if doping causes the $(C_nH_n)_mM$ structure to continuously transform to the $(C_{n+1}H_{n+1})_mM$ structure, where n is an integer. Also, the existence of chain segments of differing length, which each contain one excess electron, provides a mechanism for chain-direction charge transport, since the interchange of such segments corresponds to carrier displacement.

G. Relationships between calculated parameters

We will now use the derived geometries and charge distribution of soliton lattices to show that the geometries and charge distributions of split-soliton lattice arrays can be predicted accurately by assuming that split solitons correspond to the resonance averaging (in the valence bond sense) of structures involving conventional solitons. This resonance average corresponds to the average of geometry and charge distribution for a conventional soliton that has a 50% weighting factor for centering on the carbon atom to the left and to the right of the atom center of the split soliton. First, we have predicted the geometries and charge distributions for the $(C_7H_7)^-$ and $(C_9H_9)^-$ split-soliton lattices from these structural parameters for the $(C_7H_7)^-$ and $(C_9H_9)^-$ soliton lattices (Table VI). This is done by averaging the structural parameters for the soliton lattice with those of the same soliton lattice translated by two CH units. Second, we used the resonance averaging to calculate the geometry and charge distribution for $(C_6H_6)^-$ and $(C_8H_8)^-$, which consist of alternating solitons and split antisolitons. As illustrated in Fig. 7, this is done for $(C_6H_6)^-$ by averaging the structural parameters of a soliton lattice having alternating five carbon and seven carbon soliton-to-antisoliton separations with the structural parameters for a soliton lattice having the alternation sequence reversed, to provide first a five carbon and then a seven carbon soliton-to-antisoliton separation. In other words, two equivalent chains are averaged that are related by a mirror plane refection through a soliton center. The AM1 derived structural parameters in Table VI for $(C_5H_5)^-$ and $(C_7H_7)^-$ provide the structural parameters for such a soliton lattice copolymer. Using these procedures, we find that the predictions from the resonance average for the $(C_6H_6)^-$ and $(C_8H_8)^-$ soliton–split-soliton lattices and for the $(C_7H_7)^-$ and $(C_9H_9)^-$ split-soliton lattices agree quite well with the structural parameters directly evaluated for these lattices from the AM1 oligomer studies (Tables VII and VIII). In all cases the maximum deviation between the resonance-average structural parameters and those derived from AM1-observed charge configurations in oligomers did not exceed 0.026 electron for carbon charges, 0.039 electron for CH charges, 0.006

Å for C-C bond distances, and 0.55° for C-C-C bond angles. The average magnitude of the deviations for these structural parameters were substantially smaller. In light of the large number of independent parameters in each category (22–25) for this comparison and the fact that the comparison for a specified parameter involved either two or three oligomer derived numbers, these relatively small differences could correspond to the effects of chain ends on oligomer geometry and charge distribution.

The Table V values of carbon charge and C-C bond lengths for the $(C_7H_7)^-$ soliton lattice, which we derived from AM1 calculations, can be compared with those derived by Tanaka *et al.*[49] for $(C_7H_7)^+$. These authors used the one-dimensional tight-binding self-consistent field crystal orbital (SCF-CO) method at the level of complete neglect of differential overlap, version 2 (CNDO-2) including all valence electrons. The sum of carbon charges reported by Tanaka *et al.*[49] for $(C_7H_7)^+$ totals -0.623, which means that the hydrogens are positive on average by only 0.054, even for the cation. The maximum difference in charge on neighboring carbons that Tanaka *et al.*[49] obtained for $(C_7H_7)^+$ is only 50% of the maximum difference that we obtain from AM1 calculations on $(C_7H_7)^-$. However, a strong correlation exists between the carbon charges calculated by Tanaka *et al.* for $(C_7H_7)^+$ and those that we have derived for $(C_7H_7)^-$. This correlation is that

$$q(+) = -0.496q(-) - 0.020 ,$$

where $q(+)$ is the calculated charge for $(C_7H_7)^+$ by Tanaka *et al.*[49] and $q(-1)$ is the calculated charge from the present work for $(C_7H_7)^-$. The correlation coefficient for this equation is 0.9995 and the maximum deviation of carbon charges from the correlation is $0.004e$. Tanaka *et al.*[49] obtained bond lengths of 1.431 and 1.342 Å for neutral polyacetylene, which are reasonably close to the present AM1 values of 1.444 and 1.347 Å. Also, the bond-length alternation pattern obtained by these authors for $(C_7H_7)^+$ is basically in good agreement with the presently derived results for $(C_7H_7)^-$—which is consistent with the Table III results that show the prediction of quite similar patterns of bond alternation in the anion and cation soliton lattices. More specifically, the changes in bond lengths upon doping calculated by Tanaka *et al.*[49] for $(C_7H_7)^+$ agree to within 0.007 Å with these calculated herein by AM1 for $(C_7H_7)^-$ (Table VI). However, the bond-length alternation pattern reported by Tanaka, Okada, and Yamabe[50] for $(C_7H_7)^-$ is so dramatically different from that which the same authors report for $(C_7H_7)^+$, $(C_{11}H_{11})^+$, and $(C_{11}H_{11})^-$ that one suspects that the former contains typographical errors in the order in which bond lengths are provided. Tanaka and co-workers[49,50] utilized only one bond angle to represent all C-C-C bond angles in these soliton lattices. Also, the bond angle changes upon doping obtained by Tanaka and co-workers[49,50] are much larger than the changes in average bond angle obtained in the present work. However, the changes in C-C-C bond angle obtained by Tanaka and co-workers[49,50] show the same basic features as do the changes in average C-C-C bond angle from our calculations, at least for dopant concentrations that are physically reasonable. Specifically, these angle changes (1) are much larger in magnitude for anion lattices than cation lattices, (2) have different signs for anion and cation lattices, and (3) increase in magnitude with increasing dopant concentration.

Figure 10 graphically depicts the effects of increasing average charge density on the alternation patterns of carbon charge. Surprisingly, the same simple equation adequately represents this pattern for the $(C_9H_9)^-$, $(C_7H_7)^-$, and $(C_5H_5)^-$ soliton lattices, the corresponding split-soliton lattices, the $(C_8H_8)^-$ and $(C_6H_6)^-$ soliton–split-antisoliton lattices, and the $(C_9H_9)^+$ soliton lattice. This equation is as follows:

$$\delta q_k = -(-1)^k \delta q_1 [\cos(\pi(k-1)/p)] , \tag{3}$$

where δq_k is the deviation of carbon charge on the kth carbon in the $(C_pH_p)^-$ or $(C_pH_p)^+$ lattice from the average carbon charge per carbon. These δq_k are calculated from the charge distributions in Tables VI to VIII. The carbons are labeled with indices k so that the carbon with index 1 is the center of a soliton or split soliton. Consequently, carbon 1 lies on the mirror plane symmetry element and the index progressly increases (or decreases) without bound in moving to the right (or left) of this carbon. Equation (3) is also valid if the cyclic atom labeling scheme shown in Fig. 4 is employed, which is used in the tables. Using Eq. (3), 34 values of δq_k for $k \neq 1$ were calculated for the various lattices considered herein and the maximum deviation between AM1 derived value and Eq. (3) derived value was 0.019 of an electron charge. The analogous equation to Eq. (3) for the deviation of charge per CH unit from the average charge per CH unit also suitably describes the AM1 calculated results, within a maximum deviation of 0.026 electron. Note also that the carbon charge fluctuations calculated for $(C_{11}H_{11})^+$, $(C_7H_7)^+$, and $(C_3H_3)^+$ by Tanaka *et al.*[49] (using the SCF-CO method at the level of CNDO-2, including all valence electrons) are also in good agreement with Eq. (3). The maximum discrepancy between the results of their quantum-chemical calculations and Eq. (3) is 0.01 electrons.

In the above comparisons we have used the AM1 determined values of δq_1 to calculate, via Eq. (3), the values of δq_k for $k \neq 1$. These AM1 calculated values of δq_1 increase in absolute magnitude with decreasing value of p, but the maximum difference in values of δq_1 for different lattices ($p = 5$–9) are small (0.044 electron for carbon charge and 0.055 electron for CH charge). Furthermore, the δq_1 for carbon charge in the soliton lattices ($p = 5$, 7, and 9) and the soliton–split-antisoliton lattices ($p = 6$ and 8) are reproduced within a maximum deviation of 0.003 electron by the linear relationship: $\delta q_1 = -(0.277p^{-1} + 0.201)$. The corresponding relationship for δq_1 for carbon charge in the split-soliton lattices ($p = 7$ and 9) has only slightly different absolute values for slope and intercept: $\delta q_1 = -(0.347p^{-1} + 0.173)$. Also, the same type of relationships describe with similar accuracy the magnitude of δq_1 for CH charge as a function of p. Using the linear dependence of δq_1 on p^{-1} and Eq. (3),

charge distributions can be derived for anion lattices $(C_pH_p)^-$ for which p is integer and larger than is addressed herein by direct calculations. There is a limit to the value of p for which this approach can be applied, since the resulting calculated charge distribution does not approach the functional form appropriate at infinite p. However, the highest value of p that corresponds to a thermodynamically stable $(C_nH_n)_mM$ lattice is probably $p=16$, and the relatively short extrapolation from $p=9$ to $P=16$ is expected to provide reliable results. We will later use this approach for calculating the charge distribution for $p=12$, which is required for the analysis of carbon 1s x-ray photoelectron data.

Using the results in Table II and Tables VI-VIII, the distribution of added negative charge between carbon and hydrogen is predicted to be nearly constant (i.e., independent of p) for $(C_pH_p)^-$ soliton lattices, split-soliton lattices, and soliton–split-antisoliton lattices for p of 5, 6, 7, 8 or 9. Specifically, the AM1 calculated change in average carbon charge divided by the AM1 calculated change in average hydrogen charge upon anion lattice formation varies from 1.55 to 1.60, depending upon the anion lattice composition chosen. This ratio is slightly larger (1.75) for AM1 calculated results on the $(C_9H_9)^+$ soliton lattice.

The change in average C-C bond length upon formation of anion or cation lattices is too small to be accurately evaluated by the present calculations. However, the largest AM1 calculated change in average C-C bond length is +0.004 Å for going from neutral polyacetylene to the $(C_5H_5)^-$ soliton lattice. Also, the product of p and the average AM1-calculated change in C-C-C bond angle upon anion lattice formation varies between 13.8° and 17.0° for p of between 5 and 9. The relatively small variability in this coefficient indicates that the average C-C-C bond angle increases approximately linearly with the average negative charge per CH unit. The corresponding AM1-calculated coefficient for the $(C_9H_9)^+$ soliton lattice has opposite sign (since the average bond angle decreases) and smaller magnitude (−4.6°).

The fluctuations in C-H bond length for the anion lattice are well correlated with the fluctuations in carbon charge. Specifically, a simple proportionality describes the relationship between C-H bond length for the kth carbon (d_k) and the excess charge on that carbon compared to the average carbon charge, δq_k. This proportionality of the AM1 calculations is that:

$$d_k = d_0 + 0.025\delta q_k \ , \tag{4}$$

where d_0 is the AM1-calculated C-H bond length for neutral polyacetylene (1.104 Å). This equation predicts, within a maximum deviation of 0.0018 Å, the 32 independent AM1-calculated C-H bond lengths needed to describe the $(C_5H_5)^-$, $(C_7H_7)^-$, and $(C_9H_9)^-$ soliton lattices; the $(C_6H_6)^-$ and $(C_8H_8)^-$ soliton–split-antisoliton lattices; and the $(C_7H_7)^-$ and $(C_9H_9)^-$ split-soliton lattices. Since δq_k obeys the cosine dependence of Eq. (3), Eq. (4) means that a similar relationship can be used to describe the fluctuations in C-H bond length for all of the anion lattices that we have investigated by AM1 calculations. This equation for the $(C_pH_p)^-$ lattice is that

$$\Delta d_k = -(-1)^k \Delta d_1 [\cos(\pi(k-1)/p)] \ , \tag{5}$$

where Δd_k is the change in C-H bond length of the kth lattice carbon upon formation of the soliton lattice from neutral polyacetylene (i.e., $\Delta d_k = d_k - d_0$) and where the atom numbering index k is as in Fig. 4. The maximum observed deviation from this equation is 0.0018 Å for the seven anion lattices investigated herein. As might be expected from Eqs. (3) and (4), the deviation between AM1-calculated average C-H bond length for an anion lattice and the AM1-calculated C-H bond length in neutral polyacetylene is small (between −0.0005 and −0.0012 Å for the seven investigated anion lattices). The values of Δd_1 in Eq. (5) are positive for the split-soliton lattices and negative for the soliton lattices and soliton–split-antisoliton lattices. However, the magnitudes of Δd_1 are quite similar for the different lattices (0.0065–0.0068 Å for the $p=5$, 6, 7, and 8 soliton lattices and soliton–split-antisoliton lattices, 0.0050 Å for the $p=9$ soliton lattice, and 0.0051 and 0.0042 Å for the $p=7$ and $p=9$ soliton–split-soliton lattices, respectively).

As would be expected if C-C-C bond-angle fluctuations were dominated by carbon-carbon electrostatic interactions, the changes in C_i-C_j-C_k bond angles ($\Delta\alpha_{ijk}$) upon formation of the anion and cation lattices are proportional to the corresponding changes in $q(C_i)q(C_k)$, which is denoted $\Delta(q_iq_k)$, where q_i and q_k are the AM1-calculated charges for the C_i and C_k carbons. Correspondingly, the following equation represents the 37 different C_i-C_j-C_k bond angles for all seven of the investigated $(C_pH_p)^-$ lattices:

$$\Delta\alpha_{ijk} = 14.2\Delta(q_iq_k) + (10.1/p) \ , \tag{6}$$

where $\Delta\alpha_{ijk}$ is in degrees. The root-mean-square deviation between the angles calculated using Eq. (6) ($\alpha_{ijk} = \Delta\alpha_{ijk} + \alpha_0$, where α_0 is the bond angle for neutral polyacetylene, 122.90° from AM1 calculations) and the observed bond angles is 0.35°. The corresponding equation representing $\Delta\alpha_{ijk}$ for the $(C_9H_9)^+$ lattice is

$$\Delta\alpha_{ijk} = 5.94\Delta(q_iq_k) - (4.75/p) \ , \tag{7}$$

which provides a root-mean-square deviation between observed and calculated $\Delta\alpha_{ijk}$ of 0.073°. Although the linear dependence in Eqs. (6) and (7) of $\Delta\alpha_{ijk}$ on $\Delta(q_iq_i)$ is as expected if the bond-angle fluctuations were dominated by carbon-carbon electrostatic interactions, the different coefficients for anion and cation lattices, as well as a nonvanishing $\Delta\alpha_{ijk}$ when $\Delta(q_iq_i)$ is zero, indicate that the complete explanations for Eqs. (6) and (7) are more complicated. Nevertheless, part of the reason for the larger bond-angle fluctuations for the anion lattices compared with the cation lattices is the larger Coulombic repulsion for nearest-neighbor nonbonded carbons for the former lattices.

AM1 calculations on the anion oligomers indicates that constraining all C-C-C bond angles to be equal results in only a small increase in formation energy. For an average charge per CH or CH_2 unit of between 0.12 and

0.15 electrons, the enthalpy increase per carbon, divided by this carbon charge (in electrons), ranges between 0.24 and 0.28 kcal/mol. Correspondingly, this is about the magnitude increase in free energy per mole of $(C_pH_p)^-$ units which is predicted in this range of average carbon charge. Constraining all C-C-C bond angles to be equal in the oligomer anions does not result in more than a 0.29° change in average C-C-C bond angle compared with the case where all such bond angles are optimized

As pointed our earlier, the calculated angle between the C-H bond and the chain-axis direction in neutral polyacetylene deviates by only a small amount from 90° (by 1.0° and 0.8° from AM1 and MNDO calculations, respectively). According to the symmetries shown in Fig. 4 for the various lattices for $p=5$ to $p=9$, the C-H bond for these lattices should be exactly orthogonal to the chain-axis direction for the C-H bond attached to the carbons that are centers of solitons or antisolitons. Further evidence for this symmetry assignment and for the adequacies of the model compounds is provided by the observed near equality of H-C-C bond angles to the same carbon that is assigned as a soliton or antisoliton center in a model compound. For this purpose we have compared both MNDO-calculated and AM1-calculated angles for both soliton and split-soliton centers that cannot be equal by molecular symmetry, for both the anion and cation model compounds. The result of this comparison for nine model ions is that the root-mean-square deviation from angle equality is only 0.28°, which again indicates the relatively small error in transferring results from the model compounds to the polyacetylene lattices. This root-mean-square deviation from angle equality is much smaller than the calculated maximum difference in C-C-H bond angles to the same carbon for the $(C_pH_p)^-$ lattices investigated. For example, this maximum angle difference for the $(C_9H_9)^-$ soliton lattice is predicted to be 3.3° (based on either AM1 or MNDO calculations on $[H(CH)_{23}H]^{3-}$).

H. Relative energies of soliton and split-soliton lattices

Crystal orbital calculations using periodic boundary conditions further establish the reliability of using geometry and charge distribution from the oligomer calculations to derive the geometry and charge distribution for the soliton and split-soliton lattices. Furthermore, these calculations indicate that the energies of soliton and split-soliton lattices are nearly degenerate.

The same AM1 model was used for the periodic boundary condition calculations as for the finite-chain calculations. This program for infinite-chain calculations has been previously described[51,52] and has been successfully applied to polymers in various investigations.[53] Except for requiring a planar backbone, all geometrical parameters were fully optimized. The cutoff radius was 38 Å in the direct space summations and five points were used in the irreducible part of the Brillouin zone. Calculations were performed for the soliton lattice and the split-soliton lattice with either five or seven CH units per unit charge. The corresponding unit cells included 10 and 14 CH units, respectively, having a charge per unit cell of either 2+ or 2−.

Depending upon whether or not the initial geometry was closest to that of the soliton lattice or the split-soliton lattice, as determined using the oligomer calculation results, the energy minima corresponded to either the soliton lattice or the split-soliton lattice. Most importantly, no significantly energy difference resulted between the soliton and split-soliton lattices For example, the energy difference in the $(C_{14}H_{14})^q$ infinite-chain calculations between the soliton lattice and the split-soliton lattice for both $q=+2$ and -2 was less than 0.1 kcal/mol per 14 CH units. Considering the large unit cell subjected to full geometry optimization, this small energy difference is within calculation error. The maximum discrepancies between the results of the two infinite-chain calculations for $(C_{14}H_{14})^{2-}$ and the results derived for the corresponding soliton and split-soliton lattices using the oligomer results [see Tables VI and VIII under $(C_7H_7)^-$] were 0.005 electron for carbon charge, 0.001 Å for carbon-carbon bond distance, and 0.4° for C-C-C bond angle.

The above described observation of essentially identical energies for the soliton and split-soliton lattices are in agreement with the results of Takahashi and Fukotome[43] using the Pariser-Parr-Pople (PPP) model with unrestricted Hartree-Fock (UHF) approximation and periodic boundary conditions for 62 CH units containing two charges. These authors discussed the quasidegeneracy of a soliton lattice and a split-soliton lattice in terms of the decomposition of characteristic parameters (bond distance and charge) into nonalternating and alternating components, A_k and B_k, respectively. Hence, $X_k=A_k+B_k$, where k is the carbon or site index and X_k can be either carbon charge or carbon-carbon bond length. Takahashi and Fukutome[43] have shown that if A_k is defined as $(2X_k+X_{k+1}+X_{k-1})/4$, then the essential difference in soliton and split-soliton lattices is that the sign of the alternating component is different in these two cases. The present calculations verify this result and provide that B_k for soliton and split-soliton lattices have different signs and essentially the same magnitude [maximum discrepancy in magnitude for B_k of 0.001 Å for carbon-carbon bond distance and 0.005 electron for carbon charge from the infinite-chain calculations on $(C_{14}H_{14})^{2-}$]. Takahashi and Fukutome[43] have shown that this symmetry or near symmetry results in the quasidegeneracy of soliton lattice and split-soliton lattice energies.

As noted in Sec. III G, the average of charge distribution and geometrical parameters for a soliton lattice and the same soliton lattice shifted by two CH units provides the charge distribution and geometrical parameters for the corresponding split-soliton lattice. Also, as noted in this section, the deviation of carbon charge from average carbon charge is nearly the same in magnitude, but opposite in sign, for corresponding carbons in the soliton and split-soliton lattices. This suggests that, depending upon the geometrical relationships of polymer chains and counter ion columns, either the soliton lattice or the split-soliton lattice might become energetically preferred.

IV. COMPARISONS OF THEORY AND EXPERIMENT

Since chain-length expansion as a function of dopant level is available for alkali-metal doped polyacetylene, comparison can be made between experimental and theoretical dimensional changes as a function of charge transfer. Such comparison assumes complete charge transfer from the alkali-metal to the polymer chains, which is consistent with NMR measurements[33] on lithium-doped polyacetylene and on sodium-doped polyacetylene. Murthy, Shacklette, and Baughman [32] have shown that alkali-metal doping of polyacetylene causes a chain-length expansion and that *p*-type doping causes a chain-length contraction. This observation has been confirmed by various investigations[18,54] for alkali-metal doped polyacetylene and extensive data has been presented by Winokur *et al.*[18] for $(CHNa_y)_x$.

The above experimental observations were preceded by extended Huckel calculations by Kertesz and coworkers,[55,56] which correctly predicted a chain-length expansion for *n*-type doping and a contraction for *p*-type doping. Quantitative agreement between theory and experiment was improved by Hong and Kertesz[57] using infinite-chain MNDO calculations. However, these calculations assumed only two independent carbon-carbon bond distances and one C-C-C bond angle. As a consequence of this approximation, bond-angle oscillations and the effect of the sign of charge on bond-angle changes were not identified. Also, while the calculated fractional changes in chain-axis dimension ($\Delta L/L$) agree with those observed at low dopant concentrations, the predicted values of $\Delta L/L$ are larger than observed at high dopant concentrations.

Figure 15 shows that the present calculations provide a calculated fractional-dimension change as function of charge transfer that is in good agreement with experiment. No significant differences are observed in the calculated $\Delta L/L$ for soliton lattices and split-soliton lattices (0.42% and 0.47%, respectively, for $(C_9H_9)^-$ and 1.04% and 1.03%, respectively, for $(C_7H_7)^-$ using the parameters in Tables VI-VIII). Hence, the experimental data cannot be used to differentiate between these different lattice types. Most significantly, as already shown by the earlier calculations of Hong and Kertesz,[57] both the predicted and observed Coulombic expansion coefficient $dL/d(\ln y)$ dramatically increase above a dopant concentration of $y=0.09$. The present calculations include the effect of oscillation in local chain direction (due to a combination of bond-angle oscillation and bond-length differences for both even bonds and odd bonds), which improves the agreement at high dopant levels between observed and calculated Coulombic expansion coefficients. Including this effect provides an average calculated $dL/d(\ln y)$ between $y=0.111$ and $y=0.143$ of 19.6%, compared with the observed value of 22.2%. The approximately 0.01 shift in y between the dopant concentration corresponding to a given $\Delta L/L$ for experimental and theoretical results is likely a consequence of an uncertainty of this amount in the experimentally determined dopant concentration. Additionally, it should be noted that the chain shortening effect caused by oscillation in local chain direction might be decreased by crystal-packing effects. Hence, crystal-packing effects could somewhat increase $\Delta L/L$ as compared with calculated results for an isolated chain. While experimental data is probably not readily obtainable at atmospheric pressure for much higher dopant concentrations than shown in Fig. 15, the calculated values of Coulombic expansion coefficient at dopant concentrations higher than those observed suggest a decrease in this coefficient.

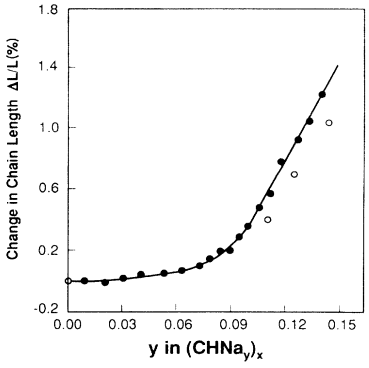

FIG. 15. Comparison of the fractional change in chain-axis dimension ($\Delta L/L$) as a function of dopant level from experiment (Ref. 18) (solid circles) and from the present theoretical analysis for sodium-doped polyacetylene (open circles).

Experimental data on $\Delta L/L$ versus y has also been presented by Winokur *et al.*[18] for polyacetylene electrochemically doped with lithium. This data shows an earlier onset of increase in Coulombic expansion coefficient than does the data on sodium doping, as well as a reduction of this coefficient to near zero at higher dopant levels. This data is not included in the present discussion, since massive solvent incorporation likely occurs during electrochemical doping with lithium, but not under these conditions with sodium, and this solvent incorporation might substantially effect experimental results. However, the polymer chains in unsolvated Li-doped $(CH)_x$ are much closer together than for larger radius alkali metals. The consequence of enhanced interchain interactions for lithium-doped $(CH)_x$ might be a reduction in the meandering of local chain direction in order to maximize packing density. In such case, $\Delta L/L$ would increase more rapidly as a function of dopant level for lithium-doped polyacetylene than for polyacetylene doped with larger alkali metals.

Comparison of observed and calculated XPS (x-ray photoelectron spectroscopic) results for sodium-doped polyacetylene provides another test of the theory. Sasai and Fukutome[58] have previously made such a comparison using experimental data from Ikemoto *et al.*[59] and theoretical results from the Pariser-Parr-Pople model with the UHF approximation. As done by Sasai and Fukutome[58] and illustrated in Fig. 16, we resolve the C1*s* XPS spectra of undoped $(CH)_x$ into a Gaussian and a residual tail component. This residual tail component has been subtracted from the spectra shown in Fig. 16 for doped polyacetylene. Using the proportionality of Siegbahn *et al.*,[60] a chemical shift (in eV, relative to neutral

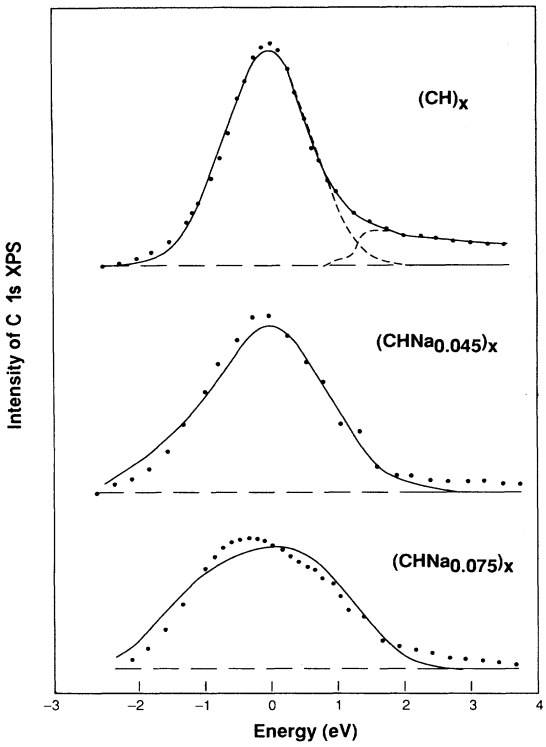

FIG. 16. Comparison of experimental (solid circles) and theoretical (solid lines) C 1*s* spectra of sodium-doped polyacetylene. The resolution of the observed spectra of undoped polyacetylene into a Gaussian and a residual tail component (which is subtracted from the observed spectra for the sodium-doped samples) is shown in the top part of this figure.

polyacetylene) of $5.6\Delta q_i$ is obtained for the C 1*s* band of a carbon having charge difference of Δq_i with respect to carbons in neutral $(CH)_x$. Correspondingly, the C 1*s* spectra of the doped composition (after subtraction of the residual tail) is provided by the sum of Gaussian curves for each of the i unique carbons, which are W_i of the amplitude of the Gaussian for undoped polyacetylene and are shifted on the energy axis by $5.6\Delta q_i$ eV with respect to the position of the Gaussian curve of undoped polyacetylene. The weighting factor W_i in this calculation is the fraction of total carbons that are the i type with charge change Δq_i.

In contrast with the present calculations, Sasai and Fukutome[58] ignore the fact that lightly doped polyacetylene is a mixture of largely undoped polyacetylene and a doped phase. These authors assume a uniform dopant concentration and apparently truncate the wings of the calculated charge distribution of an isolated soliton, so as to provide a distribution of carbons that has an average charge per CH unit corresponding to the average dopant level in the polymer. More consistent with experimental results, the present calculations assume that the doped samples of Ikemoto *et al.*[59] with $y=0.045$ and 0.075 in $(CHNa_y)_x$ are a mixture of undoped $(CH)_x$ and $(C_4H_4)_3Na$. Hence, on a carbon basis $(CHNa_{0.045})_x$ and $(CHNa_{0.075})_x$ are 46.0% and 10.0% undoped $(CH)_x$, respectively, the rest being provided by carbons in $(C_4H_4)_3Na$. The energy shifts for the Gaussian curves are calculated using Siegbahn's proportionality constant between chemical shift and carbon charge change. Such an approximation neglects the Madelung term for C 1*s* energy shift, but this is quite reasonable in light of previous experimental and theoretical work[61] on the XPS spectra of charge-transfer complexes. The changes in the charges on carbons required for calculation of the above energy shifts are obtained by adding the oscillatory component δq_i of carbon charge from Eq. (3) to the average change in carbon charge in going from undoped polyacetylene to $(C_4H_4)_3Na$. The value of δq_1 in Eq. (3) is obtained from the relationship between δq_1 and p in $(C_pH_p)^-$, where p is 12 for $(C_4H_4)_3Na$. Also, the average carbon charge in $(C_4H_4)_3Na$ is obtained from the average charge per CH in $(C_4H_4)_3Na$, 0.0833 electrons, using the fact that the ratio of AM1-calculated change in carbon charge upon doping to the similarly calculated change in hydrogen charge is very nearly 1.57. This proportionality is probably a good approximation for $(C_4H_4)_3Na$, since this ratio varies between 1.55 and 1.60 for the various AM1 oligomer calculations for the soliton, split-soliton, and soliton–split-soliton lattices.

Figure 16 shows that relatively good agreement is obtained between calculated and observed XPS spectra for both $(CHNa_{0.045})_x$ and $(CHNa_{0.075})_x$. No adjustable fit parameters are used in this comparison other than in describing the XPS spectra of undoped polyacetylene. Note that, since Eq. (3) pertains to all calculated lattice types, the present theory predicts identical XPS spectra would result for both soliton lattices and split-soliton lattices. Also, since it is shown in Sec. III A that AM1 and MNDO provide nearly the same calculated changes in carbon charge upon doping, the above calculation is insensitive to which of these methods is used.

Energy minimization calculations to predict the changes in crystal packing that result from the presently derived distortions in molecular structure are beyond the scope of the present work. However, it is interesting to note that the calculated oscillations in local chain-axis direction results in carbon displacements perpendicular to the overall chain-axis direction which are comparable to the chain translations derived from diffraction data (0.36 ± 0.08 Å for $(C_nH_n)_4K$ according to Chen *et al.*[13]). For example, carbon atoms that would coincide in chain-axis projection for a simple zig-zag chain are predicted to have a relative displacement in this projection which increases with decreasing charge density from 0.21 Å for the $(C_5H_5)^-$ soliton lattice to 0.40 Å for the $(C_8H_8)^-$ soliton–split-antisoliton lattice, and to 0.53 Å for the $(C_9H_9)^-$ soliton lattice. Also, note that the lateral positions of average charge centers for chain segments centered about successive mirror planes alternate between approximately oppositely directed deviations with respect to the average lateral charge center of the chain. For example, these lateral deviations for the $(C_8H_8)^-$ lattice (calculated from the results in Table VII) are -0.43 Å for the chain segment from C_1H_1 to C_5H_5 and $+0.38$ Å for the chain segment from C_5H_5 to C_9H_9, where the

atom labeling is as shown in Fig. 4. It is interesting that these charge center deviations are very nearly equal to the symmetry-breaking chain translation reported by Chen *et al.*[13]

Using the experimentally observed value[1] of $a'=5.99$ Å for $(C_4H_4)_2K$ and the chain shift reported by Chen *et al.*[13] of 0.36 ± 0.08 Å, a simple crystal-packing arrangement can be shown to provide both a large separation between the above defined charge centers on nearest-neighbor chains and intermolecular interatomic distances which are in the normally observed range. This packing arrangement provides neighboring chains in an a' direction which differ only in a chain-axis rotation of 180°. Such arrangement of chains with charge centers at the same chain-axis coordinate provides void extensions and contractions that alternate in the chain-axis direction. The nearest-neighbor chains to these a'-axis chains (which are perpendicular or approximately perpendicular to these a'-axis chains) can nestle between these a'-axis chains, so as to provide charge centers and outward chain bows that are midway in chain-axis coordinate with respect to those for these a'-axis chains. Except for the oscillations in chain structure and the chain displacements of about 0.3 Å normal to the chain axis, this packing arrangement is identical to that originally proposed[1] for this phase (see Fig. 1). However, present x-ray-diffraction investigations do not provide the precise nature of the structural distortions and the above simple packing arguments do not result in a unique structure solution. Consequently, further experimental work and refined energy minimization packing calculations are required in order to fully establish the nature and origin of symmetry-breaking distortions in interchain packing.

V. DISCUSSION

The present calculations provide a complete set of geometrical parameters, and related charge distributions, which are applicable to the entire dopant concentration range for which $(C_nH_n)_2M$ phases are stable. These directly calculated results are for single chain dopant concentrations from $y=0.11$, corresponding to $(C_9H_9)^-$, to $y=0.20$, corresponding to $(C_5H_5)^-$. Using these results, empirical relationships are developed that permit prediction of charge distribution and selected geometrical parameters outside of this dopant concentration range, such as for known $(C_4H_4)_4M$ and $(C_4H_4)_3M$ phases corresponding to $y=0.0625$ and $y=0.0833$, respectively. There is presently no evidence for any other thermodynamically stable alkali-metal doped phases in the compositional range from a dopant concentration near zero to $y=0.0625$, corresponding to the $(C_4H_4)_4M$ phase. Consequently, the presently derived results are applicable below $y=0.0625$, since the equilibrium doped polyacetylene consists of a mixture of largely undoped polyacetylene and the above dopant-rich phase.

The application of the present calculations over the entire dopant concentration range presumes that a transition to a polaron lattice does not occur. In contrast, Kivelson and Heeger[62] have proposed that a transition from soliton lattice to polaron lattice explains the observed[63] onset of Pauli paramagnetism at about 6% dopant level. However, the onset of a polaron lattice appears to be contradicted by experimental data.[64–67] Specifically, the intensities of the three doping-induced infrared absorption lines (associated with solitons at low dopant concentrations) increase nearly linearly with dopant concentration at all dopant levels for K-doped polyacetylene,[65] while the infrared absorption due to polarons is predicted[67] to be small and to vanish at high dopant levels. Also, electron-energy-loss spectroscopy on sodium-doped polyacetylenes by Fink *et al.*[66] indicates levels spread across the gap, which is consistent with soliton states. Additionally, the observation of intense infrared absorption lines associated with solitons up to very high dopant concentrations[65] support the present calculations, which predict that charge oscillations do not vanish.

The present calculations show that two different types of lattices are quasidegenerate for $(C_pH_p)^-$ when p is odd: the soliton lattice and the split-soliton lattice. This quasidegeneracy was also shown by Takahashi and Fukutome[43] using the PPP model with UHF approximation and periodic boundary conditions for 62 CH units containing two charges. Also, the present AM1 calculations show that $(C_pH_p)^-$ with p even provides a lattice in which solitons and split-antisolitons alternate and that such a lattice is more stable than one in which solitons and antisolitons alternate with successive separations of $p-1$ and $p+1$ CH units. Stafstrom[44] has shown that the Su-Schrieffer-Heeger Hamiltonian, including terms for π-electron hopping and σ-bond repulsion, results in similar predictions of two soliton types for p equal to 12. Also, the present AM1 calculations indicate that the geometry and charge distribution due to lattices involving split-solitons is almost precisely the average of geometry and charge distribution for two equivalent soliton lattices in which the charge centers of the two lattices have a relative displacement of two CH units. If every charge center has this displacement, the average is a split-soliton lattice, and if only every other of these charge centers has this displacement, the average provides the soliton–split-antisoliton lattice.

Since the single chain calculations provide essentially identical energies for the soliton and split-soliton lattices $(C_pH_p)^-$ when p is odd, it is possible that interchain and chain-dopant interactions will determine which of these structures is energetically preferred. More generally, it is important to determine the effect of these interactions on polymer charge distribution and geometry. *Ab initio* Hartree-Fock level calculations by Fredricksson and Strafstrom[68] and calculations by Strafstrom,[44] using a modified Su-Schrieffer-Heeger Hamiltonian, led these authors to conclude that interchain and inter-ion electrostatic interactions significantly modify soliton charge distribution and geometry. The former calculations on singly charged ions predicted a localization, while the latter calculations for multiple charged chains (using cyclic boundary conditions) predicted a delocalization. However, ^{13}C NMR results for diphenylpolyenes in solution indicate that carbon charge distribution is insensitive to the size of the counterion,[42] suggesting that the effects of

external charges on chain charge distribution might be small. Further support for the reliability of the single chain calculations is provided by the agreement between observed and calculated chain-direction Coulombic expansion and C 1*s* XPS spectra.

Based on these comparisons of theory and experiment, we suspect that the principal effect of interchain and ion-chain Coulomb interactions on chain charge distribution and geometry for commensurate lattices with high charge density will be to determine the phase of polymer structure and charge oscillations relative to that of the ion columns, and perhaps to stabilize either a soliton or split-soliton lattice for $(C_pH_p)^-$ when p is an odd integer. Likewise, when p is noninteger, so that the lattice consists of a mixture of $(C_rH_r)^-$ and $(C_{r+1}H_{r+1})^-$ segments (where $p-1<r<p$ and r is integer), we suspect that such Coulomb interactions will determine the relative locations of these segments, subject to the constraint that a segment containing an odd number of carbons must be matched on opposite sides by either a soliton and antisoliton or a split soliton and a split antisoliton. Relevant to the magnitude of interchain and ion-chain Coulomb effects, it is important to note the insensitivity of derived parameters to average charge density on the oligomer ion. While the oligomer chain length and charge does effect the calculated sequence of soliton, antisolitons, split solitons, and split antisolitons, until close to the chain ends the total amount of charge per integer number of carbons is very near unity, the symmetries expected for these charged entities are well preserved, and the oligomer calculations provide parameters that are in exceptional agreement with infinite-chain calculations. It is quite reasonable to expect that interchain and ion-chain Coulomb effects would be no more substantial than this effect of finite-chain length. These comments naturally pertain only to the case of principal practical interest where charge density is sufficiently high that solitons and antisolitons, split solitons and split antisolitons, or combinations thereof are sufficiently close together to strongly interact. In the opposite limit, explored by Fredriksson and Straftrom[44] and by Takahashi and Fukutome,[69] the effect of interchain and ion-chain Coulomb effects are expected to be more substantial. However, even here the effect of interchain Coulomb interactions partially compensated the localization caused by ion-chain interactions.[44]

The predictions of large bond-angle oscillations for the anion lattices is an important result of the present calculations. Although the origin of these fluctuations is more complicated, a partial electrostatic origin is suggested by the observation that the change in C_i-C_j-C_k bond angle upon charge transfer is linearly proportional to the change in the product of charge on the C_i and C_k carbons. Consequently, part of the reason for the larger bond-angle oscillations for the anion lattices than for corresponding cation lattices is the larger changes in this product of carbon charges for the former. The good agreement obtained between calculated and observed Coulombic chain-direction expansion as a function of alkali-metal dopant level depends upon inclusion of the partially compensating effect of oscillation in local chain-axis direction on the expansion caused by an increase in average bond angle. This oscillation in local chain-axis direction is shown to result from additive contributions due to oscillations in C-C-C bond angles and the generally unequal lengths of both even- and odd-carbon-carbon bonds. Previous calculations[57] of the Youngs modulus increase upon electron donation to polyacetylene have neglected oscillation in local chain-axis direction. Correspondingly, this increase in the Youngs modulus of a chain is most likely overestimated.

We have described in full detail the geometry and charge distribution predicted for the various investigated lattices. One of the purposes for such complete description is to provide a starting point for refinements in both comparisons of observed and calculated diffraction data and crystal-packing calculations. For example, presently available diffraction data is insufficient to directly determine more than the average of the eight independent carbon-carbon bond angles required to describe the carbon backbone in $(C_8H_8)^-$. As a consequence, previous calculations of x-ray-diffraction patterns have generally assumed only one bond angle and one bond length. In contrast with this case where all even-carbon atoms and all odd-carbon atoms coincide in chain-axis projection, carbon atom spatial deviations in this projection of up to 0.40 Å are herein predicted for $(C_8H_8)^-$, as a consequence of oscillation in local chain-axis direction. It will be interesting to see the effect of including such deviations on the chain displacements (and/or chain rotations) derived from the x-ray-diffraction data. Likewise, initial efforts to predict crystal packing by energy minimization methods have assumed all equal bond lengths and bond angles.[70,71] It will be interesting to assess in refined calculations the degree to which local bond-length oscillations are modified by crystal-packing effects and whether or not such calculations can reliably predict structural distortions consistent with the x-ray diffraction results. Such calculations, which are beyond the scope of the present work, are in progress.

ACKNOWLEDGMENTS

The authors thank J. E. Fischer, E. M. Conwell, G. Zerbi, J. Fink, K. Tanaka, T. Yamabe, A. Zakhidov, H. Fukutome, and J. L. Bredas for useful discussions concerning the present work. Work at Georgetown University has been supported by National Science Foundation (NSF) Grant No. DMR 9115548.

[1]R. H. Baughman, N. S. Murthy, and G. G. Miller, J. Chem. Phys. **79**, 515 (1983).
[2]R. H. Baughman, L. W. Shacklette, N. S. Murthy, G. G. Miller, and R. L. Elsenbaumer, Mol. Cryst. Liq. Cryst. **118**, 253 (1985).
[3]L. W. Shacklette, N. S. Murthy, and R. H. Baughman, Mol. Cryst. Liq. Cryst. **121**, 201 (1985).
[4]J. Ma, D. Djurado, J. E. Fischer, N. Coustel, and P. Bernier, Phys. Rev. B **41**, 2971 (1990).
[5]R. L. Elsenbaumer, P. Delannoy, G. G. Miller, C. E. Forbes, N. S. Murthy, H. Eckhardt, and R. H. Baughman, Synth. Met. **11**, 251 (1985).
[6]N. S. Murthy, L. W. Shacklette, and R. H. Baughman, Phys. Rev. B **41**, 3708 (1990).
[7]C. Mathis, R. Weizenhofer, G. Lieser, V. Enkelmann, and G. Wegner, Macromol. Chem. **189**, 2617 (1988).
[8]J. P. Aime, M. Bertault, P. Delannoy, R. L. Elsenbaumer, G. G. Miller, and M. Schott, J. Phys. (Paris) Lett. **46**, L379 (1985).
[9]D. Billaud, F. Saldi, J. Ghanbaja, D. Begin, and M. Lelaurain, Synth. Met. **35**, 113 (1990).
[10]F. Saldi, M. Lelaurain, and D. Billaud, Synth. Met. **41-43**, 63 (1991).
[11]P. A. Heiney, J. E. Fischer, D. Djurado, J. Ma, D. Chen, M. J. Winokur, N. Coustel, P. Bernier, and F. E. Karasz, Phys. Rev. B **44**, 2507 (1991).
[12]F. Saldi, M. Lelaurain, and D. Billaud, Solid State Commun. **76**, 595 (1990); **80**, 649 (1991).
[13]D. Chen, M. J. Winokur, P. A. Heiney, J. E. Fischer, D. Djurado, J. Ma, N. Coustel, P. Bernier, and F. E. Karasz (unpublished); D. Chen, M. J. Winokur, Y. Cao, A. J. Heeger, and F. E. Karasz, Phys. Rev. B **45**, 2035 (1992).
[14]O. Leitner, H. Kahlert, G. Leising, J. Fink, and H. Fritzsche, Synth. Met. **28**, D225 (1989).
[15]N. S. Murthy, R. H. Baughman, and L. W. Schacklette, in *Frontiers of Polymer Research,* edited by P. N. Prasad and J. K. Nigam (Plenum, New York, 1991), pp. 385–394.
[16]N. S. Murthy, L. W. Shacklette, and R. H. Baughman, Phys. Rev. B **40**, 12 550 (1989).
[17]M. J. Winokur, Y. B. Moon, A. J. Heeger, J. Barker, D. C. Bott, and H. Shirakawa, Phys. Rev. Lett. **58**, 2329 (1987).
[18]M. J. Winokur, Y. B. Moon, A. J. Heeger, J. Barker, and D. C. Bott, Solid State Commun. **68**, 1055 (1988).
[19]N. S. Murthy, R. H. Baughman, L. W. Shacklette, H. Fark, and J. Fink, Solid State Commun. **78**, 691 (1991).
[20]M. J. Winokur, D. Chen, and F. E. Karasz, Synth. Met. **41**, 341 (1991).
[21]D. Chen, M. J. Winokur, M. A. Masse, and F. E. Karasz, Phys. Rev. B **41**, 6759 (1990).
[22]L. W. Shacklette and J. E. Toth, Phys. Rev. B **32**, 5892 (1985).
[23]C. Fite and P. Bernier, Phys. Rev. B **36**, 4574 (1987).
[24]C. Fite and P. Bernier, Synth. Met. **28**, D387 (1989).
[25]P. Bernier, F. Rachdi, A. El-Khodary, and C. Fite, Synth. Met. **24**, 31 (1988).
[26]N. Coustel, P. Bernier, and J. E . Fischer, Phys. Rev. B **43**, 3147 (1991).
[27]M. Fouletier, P. Degotl, and M. B. Armand, Solid State Ionics **8**, 165 (1983).
[28]J. Tanaka, Y. Saito, M. Shimizu, C. Tanaka, and M. Tanaka, Bull. Chem. Soc. Jpn. **60**, 1595 (1987).
[29]H. Eckhardt, L. W. Shacklette, J. S. Szobota, and R. H. Baughman, Mol. Cryst. Liq. Cryst. **117**, 401 (1985).
[30]G. Zannoni and G. Zerbi, Solid State Commun. **48**, 871 (1983).
[31]S. Lefrant, E. Faulques, and A. Chentli, Synth. Met. **17**, 313 (1987).
[32]N. S. Murthy, L. W. Shacklette, and R. H. Baughman, J. Chem. Phys. **87**, 2346 (1987).
[33]P. Bernier, C. Fite, A. El-Khodary, F. Rachdi, K. Zniber, H. Bleier, and N. Coustel, Synth. Met. **37**, 41 (1990).
[34]M. J. S. Dewar and W. Thiel, J. Am. Chem. Soc. **99**, 4889 (1977); **99**, 4907 (1977).
[35]M. J. S. Dewar, E. G. Zoebisch, E. F. Healy, and J. J. P. Stewart, J. Am. Chem. Soc. **107**, 3902 (1985).
[36]G. G. Ferenczy, C. A. Reynolds, and W. G. Richards, J. Comput. Chem. **11**, 159 (1990).
[37]D. S. Boudreux, R. R. Chance, J. L. Bredas, and R. Silbey, Phys. Rev. B **28**, 6927 (1983).
[38]R. R. Chance, D. S. Boudreaux, J. L. Bredas, and R. Silbey, *Handbook of Conducting Polymers,* edited by T. A. Skotheim (Marcel Dekker, New York, 1986), Vol. 2, Chap. 24, pp. 825-857.
[39]M. Orozco and F. J. Luque, J. Comput. Chem. **11**, 909 (1990).
[40]L. M. Tolbert and M. E. Ogle, J. Am. Chem. Soc. **111**, 5958 (1989).
[41]L. M. Tolbert and M. E. Ogle, Mol. Cryst. Liq. Cryst. **189**, 279 (1990).
[42]L. M. Tolbert and M. E. Ogle, J. Am. Chem. Soc. **112**, 9519 (1990).
[43]A. Takahashi and H. Fukutome, Solid State Commun. **62**, 279 (1987).
[44]S. Strafstrom, Phys. Rev. B **43**, 9158 (1991).
[45]C. Castiglioni, M. Gussoni, M. Miragoli, and G. Zerbi, Mol. Cryst. Liq. Cryst. **117**, 295 (1985).
[46]R. H. Baughman, B. E. Kohler, I. J. Levy, and C. Spangler, Synth. Met. **11**, 37 (1985).
[47]M. J. Duijvesstijin, A. Manenschijn, J. Smidt, and R. A. Wind, J. Magn. Reson. **64**, 461 (1985).
[48]C. S. Yannoni and T. C. Clarke, Phys. Rev. Lett. **51**, 6321 (1982).
[49]K. Tanaka, M. Okada, T. Koike, and T. Yamabe, Synth. Met. **31**, 181 (1989).
[50]K. Tanaka, M. Okada, and T. Yamabe, Synth. Met. **38**, 395 (1990).
[51]J. J. P. Stewart, MOSOL Manual (United States Air Force, Colorado Springs, CO, 1984).
[52]J. J. P. Stewart, Quant. Chem. Prog. Exchange **5**, 62 (1985).
[53]See, for example, Y. S. Lee and M. Kertesz, J. Chem. Phys. **88**, 2609 (1988).
[54]O. Leitner, G. Leising, H. Kahlert, J. Fink, and H. Fritsche, in *Electronic Properties of Conjugated Polymers II,* edited by H. Kuzmany, M. Mehring, and S. Roth, Springer Series in Solid State Sciences Vol. 91 (Springer-Verlag, Berlin, 1989), pp. 42-45.
[55]M. Kertesz, F. Vonderviszt, and S. Pekker, Chem. Phys. Lett. **90**, 430 (1982).
[56]M. Kertesz, Mol. Cryst. Liq. Cryst. **126**, 103 (1985).
[57]S. Y. Hong and M. Kertesz, Phys. Rev. Lett. **64**, 3031 (1990).
[58]M. Sasai and H. Fukutome, Solid State Commun. **58**, 735 (1986).
[59]I. Ikemoto, T. Ichihara, C. Egawa, K. Kikughi, H. Kuroda, Y. Furukawa, I. Harada, and H. Shirakawa, Bull. Chem. Soc. Jpn. **58**, 747 (1985).
[60]K. Siegbahn, C. Nordling, G. Johansson, J. Hedman, P. F. Heden, K. Hamrin, U. Gelius, T. Bergmark, L. O. Werme, R. Manne, and Y. Baer, *ESCA Applied to Free Molecules* (North-Holland, Amsterdam, 1969), p. 114.
[61]W D. Grubman and E. E. Koch, Topics Appl. Phys. **27**, 261 (1979).

[62]S. Kivelson and A. J. Heeger, Phys. Rev. Lett. **55**, 308 (1985).
[63]F. Moraes, J. Chen, T. C. Chung, and A. J. Heeger, Synth. Met. **11**, 271 (1985).
[64]E. M. Conwell, H. A. Mizes, and S. Jeyadev, Phys. Rev. B **40**, 1630 (1989).
[65]D. Tanner, G. Doll, K. Rao, P. C. Eklund, G. Arbuckle, and A. G. MacDiarmid, Synth. Met. **28**, D141 (1989).
[66]J. Fink, N. Nucker, B. Scheener, A. vom Felde, and G. Leising, in *Electronic Properties of Conjugated Polymers,* edited by H. Kuzmany, M. Mehring, and S. Roth (Springer-Verlag, New York, 1987), p. 94.
[67]H. Y. Choi and E. J. Mele, Phys. Rev. B **34**, 8750 (1986).
[68]C. Fredriksson and S. Stafstrom, Synth. Met. **44**, 65 (1991).
[69]A. Takahashi and H. Fukutome, Synth. Met. **28**, D469 (1989).
[70]D. A. Morton-Blake, Synth. Met. **35**, 281 (1990).
[71]J. Corish, V. C. A. Hanratty, J. P. Margrita, D. A. Morton-Blake, F. Beniere, and A. Morin, J. Mol. Struct. (Theochem.) **207**, 53 (1990).

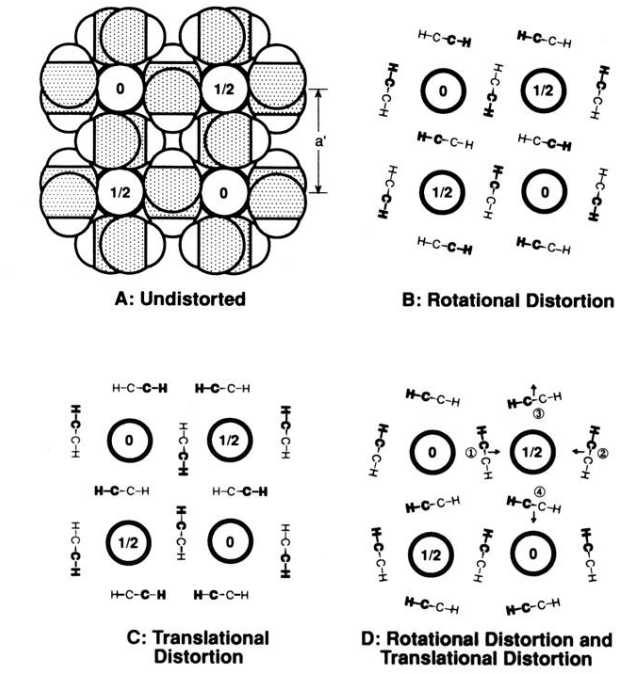

FIG. 1. Chain-axis projections for various structural models for the tetragonal or pseudotetragonal $(C_nH_n)_4K$ phases. In the representation used for model A, which shows van der Waals dimensions for all atoms, the carbons correspond to the dot-highlighted circles and the small intersecting circles correspond to the attached hydrogens. The columns of potassium ions are shown in all models as the circles having the van der Waals radius of K^+ and a number to indicate the relative chain-axis heights of neighboring ion columns for a body centering of columns.

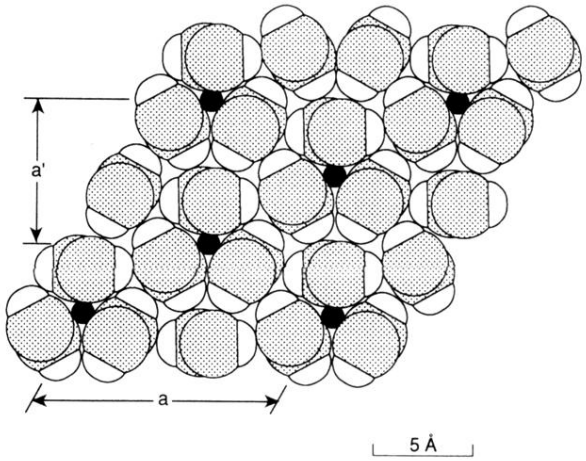

FIG. 2. Chain-axis projection for the structural model proposed by Murthy, Shacklette, and Baughman (Ref. 14) for Li-doped polyacetylene. The structure is hexagonal or pseudohexagonal. The indicated a' is a unit-cell parameter that provides the periodicity in chain-axis projection and the larger unit-cell parameter a corresponds to the basal-plane unit-cell parameter for the three-dimensional structure.